J Comput Neurosci
DOI 10.1007/s10827-014-0508-6

Adaptation and shunting inhibition leads to pyramidal/interneuron gamma with sparse firing of pyramidal cells

Martin Krupa · Stan Gielen · Boris Gutkin

Received: 15 April 2012 / Revised: 29 May 2014 / Accepted: 2 June 2014

Abstract Gamma oscillations are a prominent phenomenon related to a number of brain functions. Data show that individual pyramidal neurons can fire at rate below gamma with the population showing clear gamma oscillations and synchrony. In one kind of idealized model of such weak gamma, pyramidal neurons fire in clusters. Here we provide a theory for clustered gamma PING rhythms with strong inhibition and weaker excitation. Our simulations of biophysical models show that the adaptation of pyramidal neurons coupled with their low firing rate leads to cluster formation. A partially analytic study of a canonical model shows that the phase response curves with a near zero flat region, caused by the presence of the slow adaptive current, are the key to the formation of clusters. Furthermore we examine shunting inhibition and show that clusters become robust and generic

Action Editor: N. Kopell

M. Krupa (✉)
Project Team MYCENAE, INRIA Paris-Rocquencourt
Research Centre, Domaine de Voluceau BP 105,
78153 Le Chesnay cedex, France
e-mail: maciej.p.krupa@gmail.com

S. Gielen
Huygens Gebouw, Radboud University Nijmegen,
Heyendaalseweg 135, 6525 AJ Nijmegen, The Netherlands

B. Gutkin
Group for Neural Theory, École Normale Superieure,
29, rue d'Ulm, 75005 Paris, France

B. Gutkin
National Research University Higher School of Economics,
Center for Cognition and Decision Making, Moscow, Russia

Keywords Gamma oscillations · Spike frequency adaptation · Clustered oscillations · Multiple timer scales · Shunting inhibition

1 Introduction

The gamma rhythm is ubiquitous in the cortex. It appears during sensory and cognitive tasks and has been associated with increased attention (Engel et al. 2001), with sensory processing and feature binding, (Gray 1999; Fries et al. 2001), with short memory formation (Tallon-Baudry et al. 1998) as well as with a range of other forms of neuronal information processing, see Wang (2010) for a review. This gamma band activity appears to be spatially organized with local coherence (von Stein and Sarnthein 2000; Jia et al. 2011).

Two regimes of gamma have been observed: strong gamma, where the pyramidal cells and fast-spiking, parvalbumin-positive basket cells fire on every cycle, and weak gamma, where interneurons fire on every cycle and pyramidal cells skip cycles (randomly), so that the individual pyramidal cell firing is sparse and yet the population shows clear gamma oscillations (Börgers et al. 2005). In an idealized and simplified model of weak gamma the pyramidal cells fire in clusters, with synchrony within each cluster (Kilpatrick and Ermentrout 2011).

One of the prevalent mechanisms of gamma is Pyramidal Interneuron Gamma (PING), based on the idea that excitatory input from the pyramidal cells to the interneurons plays an important role in the formation of the rhythm (Whittington et al. 1997; Cunningham et al. 2004). The overall scheme for PING (weak or strong) is as follows: the pyramidal cells fire a volley of spikes, strongly exciting the inhibitory interneurons, whose firing, in turn, suppresses the

Published online: 09 July 2014

pyramidal cell activity. When the inhibition wears off, the pyramidal cells are free to fire a volley again. Theoretical analyses have shown (Börgers and Kopell 2003, 2005) that such ping-pong of excitation and inhibition should lead to synchronization. The difference between weak and strong PING is that, in strong PING, the pyramidal cells fire in synchrony (all approximately at the same time), while in weak PING only a subset of the pyramidal cells fire at a time. Thus the mechanisms that lead to PING synchronization are a combination of intrinsic cellular properties and synaptic properties. The focus of earlier work on strong gamma (Börgers and Kopell 2003, 2005) has been on the synaptic properties, specifically on the role of inhibition in timing the gamma oscillations. While gamma synchrony is generically global, several works have shown that the firing of individual pyramidal cells can have much lower frequency than gamma (Cunningham et al. 2004). Some of the time traces of experimental data indicate that the pyramidal cells could be firing regularly, in particular this is suggested by Fig. 1 in Cunningham et al. (2004).

The spatial organization of weak gamma remains a question of interest. An important advance in understanding weak gamma came through the work of Kilpatrick and Ermentrout (2011) who showed using methods of singular perturbation theory that a combination of inhibition and spike frequency adaptation can lead to clustered firing of pyramidal cells. These authors derived an asymptotic formula for the number of clusters depending on the strength and the duration of the adaptation current. Formally speaking, the mechanism of the formation of clusters depends on the skewed shape of the Phase Response Curve (PRC). The strength and the duration of adaption influence the shape of the PRC and thus play an important role in the formation of clusters (weak gamma). We also mention earlier work on clustered solutions in networks with inhibitory connections (Golomb and Rinzel 1994).

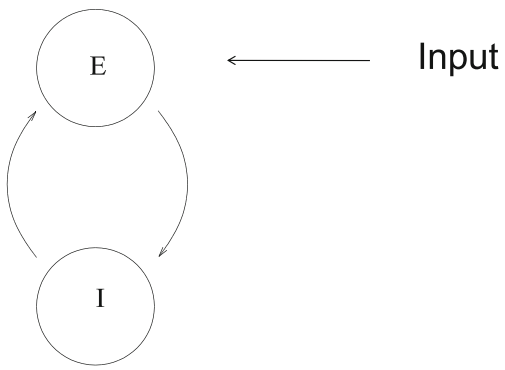

Fig. 1 Schematic drawing of the PING model consisting of a population of E-cells (E with a circle around it) and I cells (I with a circle around it)

The article of Kilpatrick and Ermentrout (2011) focuses on the very important role of the adaptation current but does not discuss the role of inhibition. In particular, their formula does not include either the strength or the duration of inhibition. On the other hand simulations show that by increasing either of these parameters while fixing the parameters of the adaptation current can significantly lower the number of clusters. In this article we explore the combined effects of adaptation and inhibition in a PING model with strong inhibition and relatively weak excitation. In particular, we obtain an estimate for the number of clusters which depends on the parameters of both the adaptation and the inhibition. We also emphasize the role of shunting inhibition, whose importance has been pointed out in the context of ING (Vida et al. 2006).

Under weak gamma conditions the pyramidal cells with adaptation have significantly skewed PRC (Ermentrout et al. 2001; Gutkin et al. 2005). We use this fact to formulate a canonical model with a coupling function which is not very close to 0 only for a short interval of the phase. In this context we explore the role of inhibition which is 'slow' in absolute time terms, but fast relative to the period of the pyramidal cells with adaptation. In this way our paper builds on the ideas of Börgers and Kopell (2003, 2005) and can be seen as a continuation of these papers. We test the derived estimate of the number of clusters with simulations of the canonical model and of a conductance based model. We also analyze the effect of the inhibitory reversal potential and find that for shunting inhibition clustering arises for weaker adaptation currents and inhibition and oscillations with many clusters are more likely to occur. We back up our simulations of conductance based models with analysis of a canonical model. Once again we reiterate that the new contribution of the paper is to consider parameters of inhibition and adaptation together in determining how gamma oscillations cluster. The feature established by Kilpatrick and Ermentrout (2011) is that adaptation currents promote clustering. The message of this paper is complementary: strong inhibition counter-acts clustering and there is more clustering when inhibition is shunting than when it is hyperpolarizing.

The paper is organized as follows. In Section 2 we introduce the biophysical model, consisting of a network of reduced Miles-Traub neurons (MT) as pyramidal cells and Quadratic Integrate and Fire neurons (QIF) as interneurons. (By choosing QIF neurons we opt for a simple model, which will not introduce extra complications to the already complex dynamics.) Next we describe our canonical model, which is a network with pyramidal cells as phase oscillators and the skew effect formally built in as an interaction function. We begin Section 3 by presenting the principal simulation results for the biophysical model. Our simulations show that spike frequency adaptation leads to clustered

gamma under strong coupling and that the number of clusters and the sparsity of firing increase when the adaptation current becomes stronger. We give a heuristic argument explaining how adaptation and low firing rate for the individual pyramidal cells lead to the clustering. Subsequently, in the context of the canonical model, we derive an estimate for the maximal number of clusters and the maximal firing period of the pyramidal cells, depending on the parameters of the canonical model. Finally we discuss shunting inhibition. Simulations for the biophysical model and for the canonical model show the clustering arises for a much larger range of adaptation currents when inhibition is shunting. Hence shunting makes out of cluster gamma a generic phenomenon. We end the paper with a discussion section.

2 Materials and methods

In this computational study we consider networks consisting of a population of excitatory (E) cells and inhibitory (I) cells, known as PING networks, see Fig. 1.

The E-cells are meant to represent pyramidal cells and the I-cells are meant to represent interneurons. The acronym PING stands for Pyramidal Interneuron Gamma. Gamma oscillations can arise in a PING model as a result of the interplay between the excitation from the E-cells to the I-cells and the inhibition from the I-cells to the E-cells. We refer to the work of Börgers and Kopell (2003) for an explanation of this phenomenon. In the present work we use PING models with two kinds of E-cells, reduced Miles-Traub (MT) cell with adaptation (AHP current) and a phase model with a specially designed coupling function (PRC). In both cases the I-cells are represented by QIF neurons.

2.1 The MT cells

The MT cell model used in this work is given by the following system:

$$\begin{aligned}\frac{dv}{dt} &= I_{\text{app}} - I_L - I_K - I_{Na} - I_{Ca} - I_{AHP}\\ \frac{dn}{dt} &= \alpha_n(v)(1-n) - \beta_n(v)n\\ \frac{dCa_2}{dt} &= -\varepsilon_{Ca} I_{Ca} - Ca_2/\tau_{Ca}.\end{aligned} \tag{1}$$

with I_{app} representing the external drive, I_L the leak current and I_{Na}, I_K are the usual spike generating sodium and potassium currents and I_{AHP} is a hyperpolarization activated, calcium dependent potassium current. Without the AHP current the equation is as in Börgers et al. (2005). The AHP current is as introduced in Jeong and Gutkin (2007).

The currents appearing in the RHS of Eq. (1) were defined as follows: $I_L = g_L(v - E_L)$, $I_K = g_K n^4(v - E_K)$, $I_{Na} = g_{Na} m_{\text{inf}}(v)^3 F_h(n)(v - E_{Na})$ and $I_{AHP} = g_{AHP}(Ca_2/(Ca_2 + 1))(v - E_K)$. The functions were defined as follows: $m_\infty(v) = \alpha_m(v)/(\alpha_m(v) + \beta_m(v))$, $\alpha_m(v) = 0.32(v+54)/(1-e^{-(v+54)/4})$, $\beta_m(v) = 0.28(v+27)/(e^{(v+27)/5} - 1)$ and $F_h = \max\{1 - 1.25n, 0\}$. The variable n measures the activation of the potassium current I_K, with $\alpha_n(v) = 0.032(v + 52)/(1 - e^{-(v+52)/5})$ and $\beta_n(v) = 0.5e^{-(v+57)/40}$. The variable Ca_2 corresponds to the calcium concentration and the calcium current is given by $I_{Ca} = g_{Ca} m_{\text{inf},1}(v)(v - E_{Ca})$, with $m_{\infty,1}(v) = 1/(1 + e^{-(v+25)/2.5})$. The following parameters were fixed throughout the computation $g_{Na} = 100$, $g_K = 80$, $g_{Ca} = 1$, $g_L = 0.1$ (in mS/cm^2), $E_L = -67$, $E_{Na} = 50$, $E_K = -100$ $E_{Ca} = 120$ (in mV), and $\tau_{Ca} = 80$ ms, $\varepsilon_{Ca} = 0.002$ (in μM (ms μA)$^{-1}$cm^2). In our simulations we omitted the I_{Ca} current in the current balance equation as its presence seemed to have no qualitative effect on the presence of clustering. The maximal conductance of the adaptation current, g_{AHP} and the external drive I_{app} were varied, as reported in the article. The AHP current has the effect of extending the relative refractory period. This means that the neuron does not respond to input in the early stage of the cycle. This feature is reflected in the PRC, which is almost 0 in the first part of the cycle, see Fig. 2, panel A, showing the PRC with three different values of g_{AHP}.

2.2 The MT PING model

The MT PING model is a network consisting of a population of MT cells (E-cells) and a population of QIF neurons (I cells), given by the following system of equations:

$$\begin{aligned}\frac{dv_{e,j}}{dt} &= I_{\text{app}} - I_L(v_{e,j}) - I_K(v_{e,j}, n_j) - I_{Na}(v_{e,j}, n_j)\\ &\quad - I_{Ca}(v_{e,j}) - I_{AHP}(v_{e,j}, Ca_{2,j})\\ &\quad - g_{ee}\left(\frac{1}{N_e}\sum_{k=1}^{N_e} s_{e,k}\right)(v_{e,j} - E^{ei}_{rev})\\ &\quad - g_{ie}\left(\frac{1}{N_i}\sum_{k=1}^{N_i} s_{i,k}\right)(v_{e,j} - E^{ei}_{rev})\\ \frac{dv_{i,l}}{dt} &= 2v_{i,l}(v_{i,l} - 1) + I_{int}\\ &\quad - g_{ei}\left(\frac{1}{N_e}\sum_{k=1}^{N_e} s_{e,k}\right)(v_{i,l} - E^{ie}_{rev})\\ &\quad - g_{ii}\left(\frac{1}{N_i}\sum_{k=1}^{N_i} s_{i,k}\right)(v_{e,j} - E^{ii}_{rev})\end{aligned} \tag{2}$$

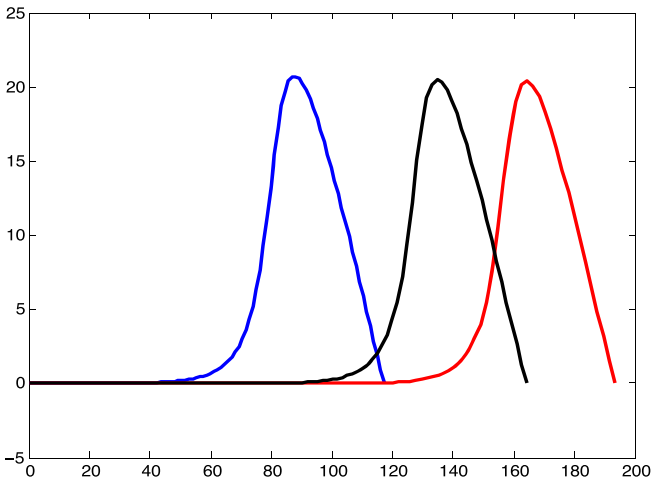

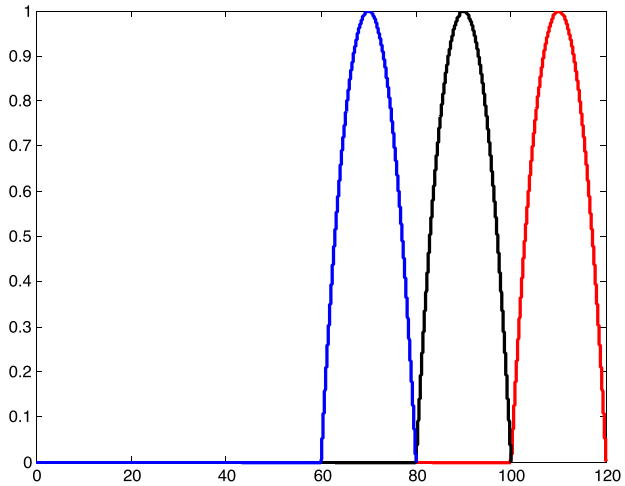

Fig. 2 **A** PRC of the Miles-Traub model with $I = 0.8$ and with different strengths of the AHP current, $g_{AHP} = 0.5$ (*blue curve*), $g_{AHP} = 1$ (*black curve*) and $g_{AHP} = 1.5$ (*red curve*), respectively. The MT cell has an inactive phase, at the beginning of the cycle (after the spike), and an active phase, at the end of the cycle. This is reflected in the PRC which is almost 0 in the early stage of the cycle and is bell shaped at the end of the cycle. As g_{AHP} increases the flat part is longer, while the bell-shaped part remains almost unchanged. **B** The graph of the coupling function $f((\theta-1)/\omega + T_0)$ of Eq. (3) plotted along the solution $\theta(t) = \omega t$, which exists in the absence of inhibition.The values of ω corresponding to different colors are $\omega = 0.0125$ (*blue*), $\omega = 0.01$ (*black*) and $\omega = 1/120$ (*red*)

with $j = 1, \ldots N_e$ and $l = 1, \ldots N_i$. The variables $v_{i,j}$ (dimensionless) varied between 0 and 1 and were reset to 0 when they reached 1 (this corresponds to a spike). The synaptic variables $s_{e,k}$ (respectively $s_{i,k}$) vary between 0 and 1. They were set to 1 after each spike of the corresponding E-cell (respectively I-cell) after a delay δ_E (respectively δ_I) and decayed exponentially with time constant τ_E (respectively τ_I). The values of the delays were $\delta_E = \delta_I = 1ms$ and the values of the time constants were $\tau_E = 1ms$ and $\tau_I = 9ms$. The maximal conductances of the synaptic currents varied; g_{ii} and g_{ie} between 1 and 2, g_{ei} between 0.1 and 0.2 and g_{ee} between 0 and 0.05. The reversal potential E^{ei}_{rev} was either -80 mV (hyperpolarizing inhibition) or -65 mV (shunting inhibition). The values of the other reversal potentials were: $E^{ee}_{rev} = 50$ mV, $E^{ie}_{rev} = 6.5$, $E^{ii}_{rev} = -0.25$. N.B. The latter two reversal potentials are for synapses onto the QIF model of the inhibitory inter-neuron, where the voltage is a non-dimensionalized variable. Hence the reversal values are also non-dimensional and are scaled with respect to the corresponding biophysical values. The value of the drive to the I-cells was $I_{int} = 0.5$ (corresponding to the saddle-node bifurcation). Since the role of interneurons in our model is intended to be very simple, and a QIF neuron is one of the the simplest models of excitable cells, we decided to use a network of QIF neurons.

2.3 PING with phase oscillators as E-cells (phase PING)

As a toy model we used a PING network with E-cells given by phase oscillators, defined by the following equations:

$$\begin{aligned}
\frac{d\theta_l}{dt} &= \omega - g_{ie} f((\theta_l - \theta_{\text{left}})/\omega)\left(\frac{1}{N_i}\sum_{j=1}^{N_i} s_{l,j}\right)\\
\frac{dv_j}{dt} &= 2v_j(v_j-1) + I_0 - g_{ei}\left(\frac{1}{N_e}\sum_{i=1}^{N_e} s_{e,i}\right)(v_j - E^{ie}_{rev})\\
&\quad - g_{ii}\left(\frac{1}{N_i}\sum_{l=1}^{N^I} s_{i,l}\right)(v_j - E^{ii}_{rev}),
\end{aligned} \tag{3}$$

with θ_l and v_j reset to 0 after reaching 1 (corresponding to a spike), $l = 1, \ldots N_e$, $j = 1, \ldots N_i$ The treatment of the synaptic variables was the same as for MT PING. The maximal synaptic conductances had the following values: $g_{ii} = 0.5$, $g_{ei} = 0.2$, with g_{ie} used as a parameter. The constant θ_{left} is defined as

$$\theta_{\text{left}} = 1 - \omega T_0, \tag{4}$$

where T_0 is set to 20 ms. The meaning of θ_{left} and T_0 will be discussed in Section 3.2.

In the absence of the coupling term θ_l is a phase oscillator, with frequency ω. As we will argue later changing ω has the same effect as changing g_{AHP}. We assume that $f(t)$ is positive on an interval $(0, T_0)$ and equal to 0 elsewhere. In addition we assume that $f'(t)$ is monotonically decreasing for $t \in (0, T_0)$; these assumptions imply the existence of a unique maximum at some $t_M \in (0, T_0)$. In a rigorous phase reduction the coupling function is the PRC of the oscillator to which the reduction is applied. Here we choose an idealized coupling function whose form is motivated by the PRCs of the Miles-Traub model; more specifically, if g_{AHP} is increased the period of the oscillation increases, but the length of the time interval in which the PRC is significantly different from 0 remains approximately constant, see Fig. 2, panel A. Similarly, if we change ω in Eq. (3), the period of the solution existing in the absence of inhibition increases but the time interval when the coupling function is active stays constant, see Fig. 2, panel B.

The first component of Eq. (3) is similar to the phase model of *oscillator death* used by Ermentrout and Kopell (1990) to model a transition from oscillation to equilibrium behavior. In our model this transition is transient and corresponds to the action of inhibition; after inhibition has sufficiently worn off the system returns to the oscillatory state.

We have also considered the modified phase PING model to mimic the effect of shunting inhibition. This modification consisted of multiplying the coupling term in the RHS of the θ_l equation by the following sigmoidal function:

$$\sigma(\theta) = \frac{1}{1 + \exp(20(0.9 - \theta))}. \tag{5}$$

Note that $\sigma(\theta)$ close to 0 in the initial part of the cycle and near 1 for θ near 1. This idea of modeling shunting inhibition was already introduced in Jeong and Gutkin (2007) and is based on the following observation. The voltage variable of the Miles-Traub cell with adaptation increases very slowly in the initial part of the cycle but becomes much faster as it passes near the value of the inhibition reversal potential, so that inhibition grows very quickly from 0 to to a near maximum value in the last stage of the cycle.

3 Results

3.1 MT PING

3.1.1 Simulations with hyperpolarizing inhibition

Börgers and Kopell (2003) describe gamma oscillations in PING models for which both the E-cells and the I-cells oscillate in synchrony at gamma frequency. The fundamental assumption of PING is that the rhythm is driven by external input coming into the E-cells and that the I cells do not receive enough drive to fire at gamma frequency. The mechanism of the oscillation can be briefly described as follows. The E-cells fire first and excite the I-cells. Excitation from the E-cells causes spikes of the I-cells, releasing a volley of inhibition. As a result no cells in the network can fire until the inhibition has sufficiently decayed. Inhibition not only delays the next spike but also synchronizes the population of the E-cells and leads to a tighter synchrony in the I-cells.

On the other hand it is known from some experiments that pyramidal cells can fire at a much lower frequency than the frequency of the rhythm (Cunningham et al. 2004). The simplest way that this can occur is if the pyramidal cells fire in clusters. Here we identify one mechanism how such firing in clusters can come about, namely a long refractory period of the E- cells (inactive phase). In our MT model this is caused by the AHP current. The main idea behind our work is that E-cells spike very slowly, so that their period is much larger than the time constant of inhibition, and that the cells are not sensitive to input in the early phase of of the cycle, so that the synchronization effect is present for a part of the phase only.

In Fig. 3 we show some simulations of clustered MT PING. The first of the two raster plots shows a solution with two clusters, with $I = 7$, $g_{ie} = 1.5$ and $g_{AHP} = 1.2$. The solution is obtained from an initial condition of the MT cells distributed evenly in the phase of their uncoupled oscillation with $I = 7$ and $g_{AHP} = 1.2$. The panel on the right shows a similarly obtained solution, now with three clusters, for $g_{AHP} = 2.3$. This example supports the results of Kilpatrick and Ermentrout (2011) that increasing g_{AHP} leads to the occurrence of more clusters.

The effect of varying inhibition is the main focus of this work. In Section 3.2, in the context of phase PING we give some analytic results illustrating this effect. In the context of MT PING our evidence consists of simulations, see Fig. 4, where we show that the number of clusters can significantly decrease if g_{ie} is decreased. In order to better explain this effect, based on heuristic considerations, we design an expression which approximates the the maximal number of clusters (see Eq. (6)), and discuss its dependance on g_{ie}. Our numerical computations (see Figs. 7 and 8), give a comparison of the predictions (6) and the changes in the number of clusters obtained by direct simulation.

The effect of changing g_{AHP} is illustrated in Fig. 3 as well as in Fig. 5, panels A and B.

Another parameter strongly influencing the number of clusters is I_{app} (the drive to the E-cells). Our simulations

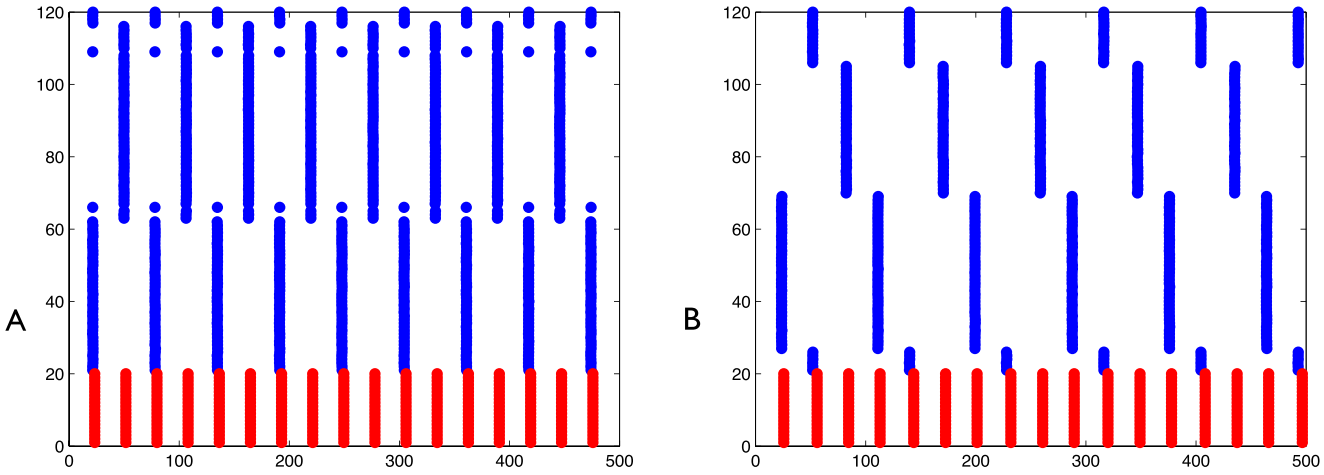

Fig. 3 Clustered gamma oscillations of the PING model with hyperpolarizing inhibition for the maximal conductance of inhibition $g_{ie} = 1.5$ and the drive to the E-cells $I = 7$. **A** A solution with two clusters, corresponding $g_{AHP} = 1.2$ (maximal conductance of the AHP current). **B** A solution with three clusters, corresponding $g_{AHP} = 2.3$

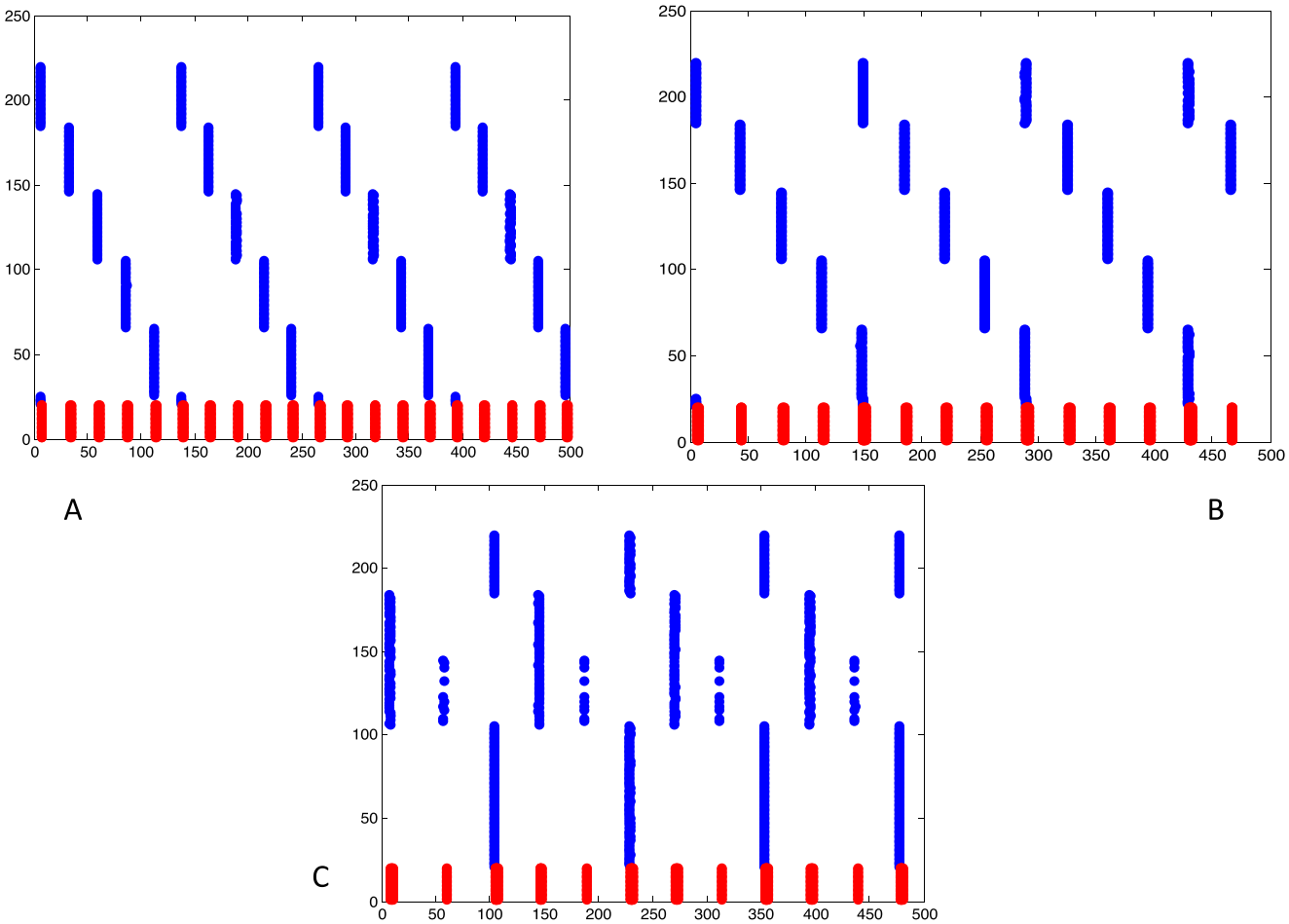

Fig. 4 Increased inhibition leads to the reduction of the number of clusters. **A** Five clusters with $I = 4$, $g_{AHP} = 2.3$, $g_{ie} = 0.5$. **B** Four clusters with $I = 4$, $g_{AHP} = 2.3$, $g_{ie} = 1.8$. **C** Three clusters with $I = 4$, $g_{AHP} = 2.3$, $g_{ie} = 1.8$

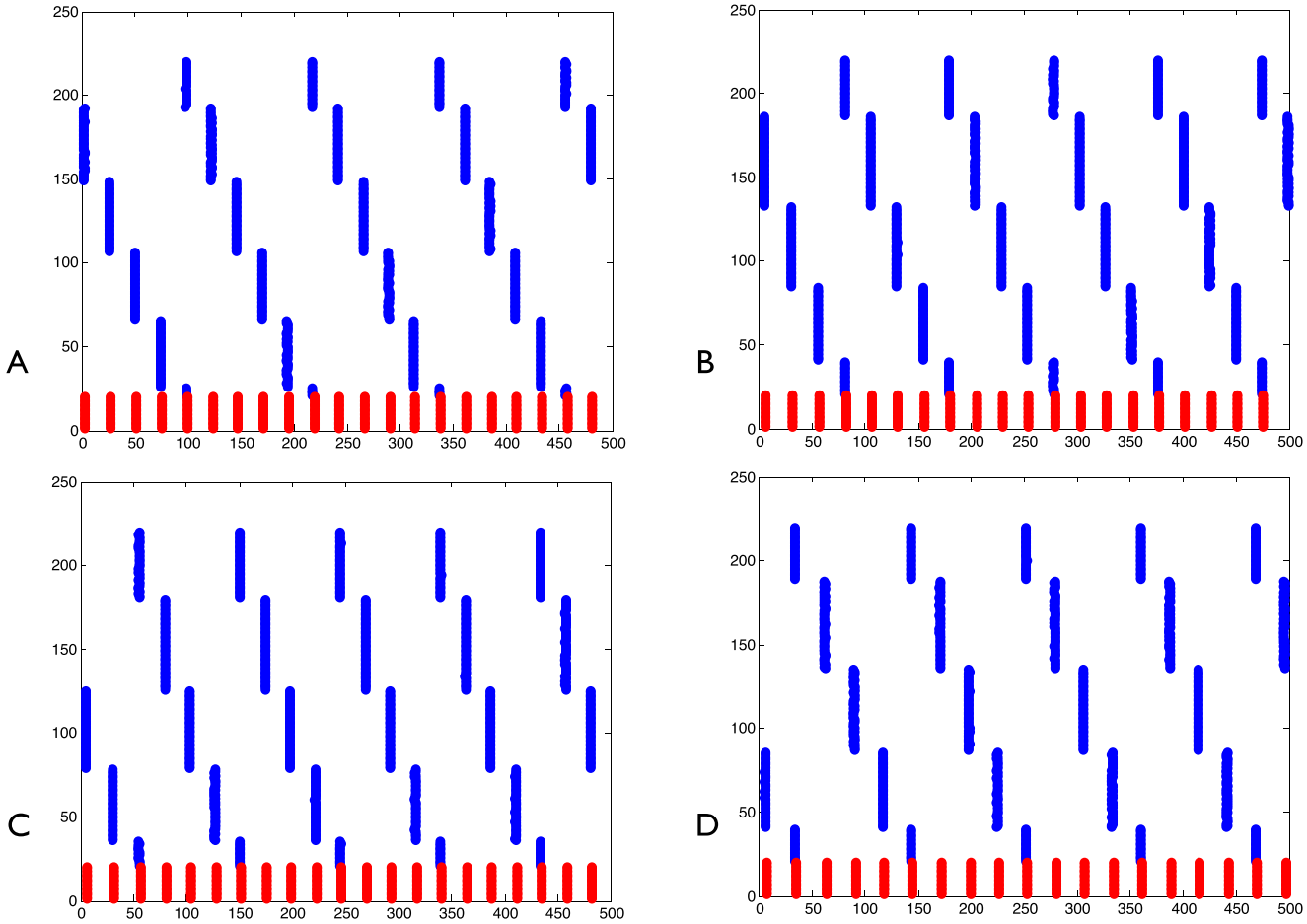

Fig. 5 The effect of changing g_{AHP}, I and g_{ei}. All solutions are computed starting from the same initial condition. **A** A five cluster solution for $g_{\mathrm{AHP}} = 2$, $I_{AHP} = 4$ and $g_{ei} = 0.3$. **B** A four cluster solution for $g_{\mathrm{AHP}} = 1.5$, $I_{AHP} = 4$ and $g_{ei} = 0.3$. **C** A four cluster solution for $g_{\mathrm{AHP}} = 2$, $I_{AHP} = 5$ and $g_{ei} = 0.3$. **D** A five cluster solution for $g_{\mathrm{AHP}} = 2$, $I_{AHP} = 4$ and $g_{ei} = 0.2$

show that raising I_{app} decreases the number of clusters see Fig. 5, panels A and C. Our heuristic argument in support of this point is as follows: if I_{app} is increased then T decreases as well as the refractory period introduced by the AHP current. Hence inhibition has a simultaneous effect on a larger portion of the cells, leading to fewer clusters (see below for an explanation of this point using the 'river picture').

Finally, the number of clusters is also controlled by g_{ei}, i.e. the strength of the projection from the E-cells to the I-cells. If g_{ei} is small then many E-cells have to spike approximately at the same time to produce a spike of the I-cells. This rules out the possibility of small clusters. Figure 5, panels A and D, shows that decreasing g_{ei} can lead to the occurrence of fewer clusters.

The main goal of this paper is to study the combined effect of inhibition (controlled by g_{ie}) and adaptation (controlled by g_{AHP}) on the existence and stability of clustered solutions. To understand the role of g_{AHP} and g_{ie} we have computed the time-to-spike function TTS, which is defined as follows. Let $t^* \in [0, T]$ be the time elapsed from the last spike of the spiking solution of the MT cell, with T corresponding to the period. Then $TTS(t^*)$ is the time it takes to the next spike given that a pulse of slowly decaying inhibition was applied at t^*. In Fig. 6 we show the graphs of TTS corresponding to the parameter values of Fig. 4.

Some properties of the TTS function in relation to the parameter g_{ie} can be easily deduced. If $g_{ie} = 0$ then $TTS(t) = T - t$, i.e. the graph of TTS is a straight line with slope -1. For $g_{ie} > 0$ the slope is strictly between -1 and 0 and becomes close to 0 in the final stage of the cycle, where the PRC is positive and therefore the 'river argument' of Börgers and Kopell (2003) implies that the time of spike is almost constant, equal to some constant T_{min} (the river argument will be reviewed in Section 3.2). At the very end of the cycle, due to the finite width of the spike, the TTS function drops sharply to 0. The TTS function is

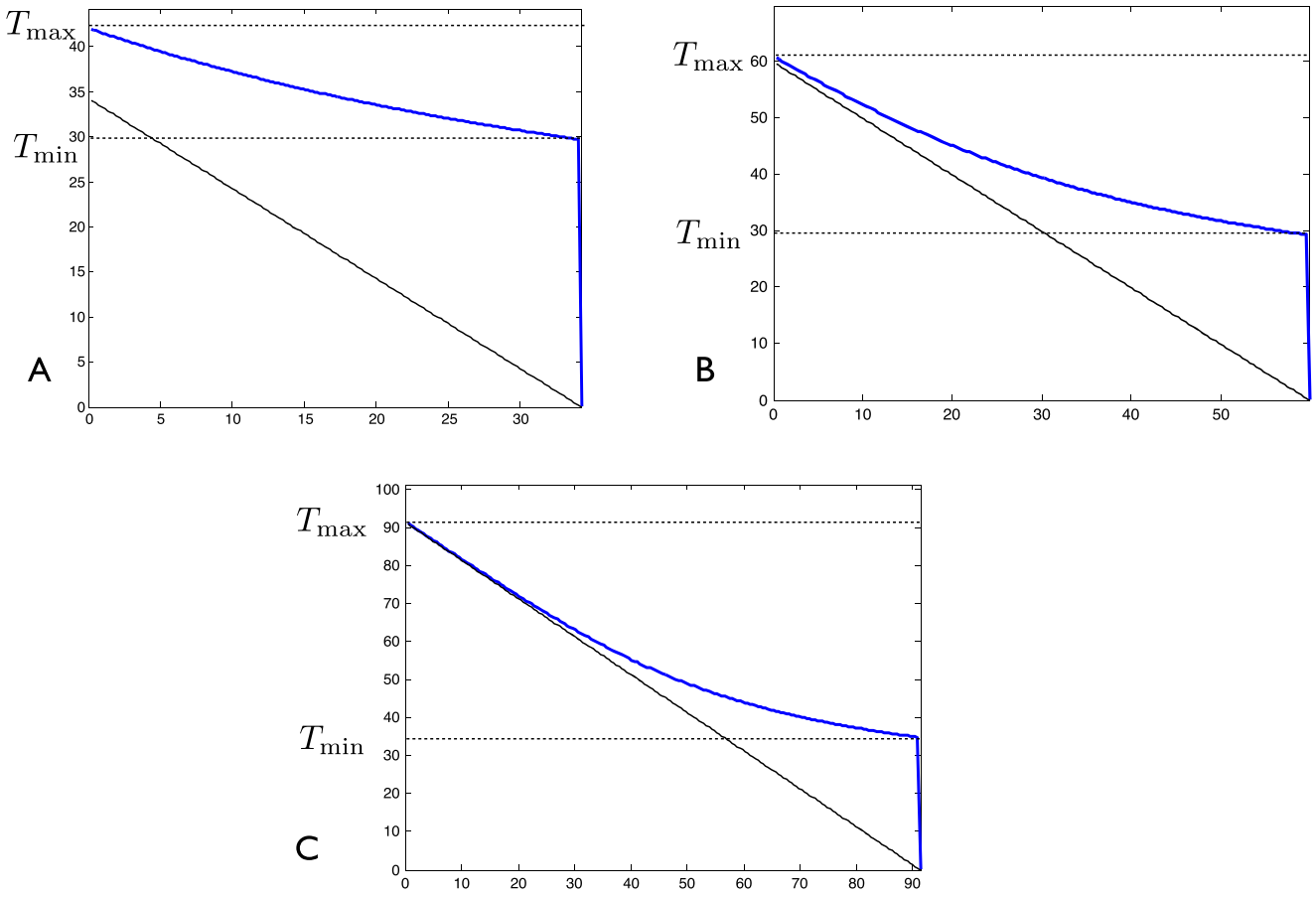

Fig. 6 Time-to-spike (TTS) function for the MT cell with adaptation. The TTS function (*blue curve*) assigns to the phase of the cell (wrt the natural period) the time to the next spike given that a pulse of inhibition arrives at the given value of the phase. For larger values of g_{AHP} the TTS function is close to the function $h(t) = T - t$ (*black line* with slope -1) at the earlier stage but its slope becomes much closer to 0 at the later stage, indicating contraction.This feature leads to a higher level of clustering, see Fig. 3. **A** TTS function with $g_{AHP} = 1.2$, $g_{ie} = 1.5$ and $I = 7$. **B** TTS function with $g_{AHP} = 2.3$, $g_{ie} = 1.5$ and $I = 7$. **C** TTS function with $g_{AHP} = 2.3$, $g_{ie} = 1.5$ and $I = 4$

decreasing, hence its maximal value $T_{\max}$ corresponds to $t^* = 0$. Our heuristic picture of the clustering is as follows. Different E-cells can be identified with the different time instances along the oscillation of the MT cell without inhibition. Suppose we divide the interval $[0, T_{\max}]$ into intervals of length $T_{\min}$, starting from the right. All the cells that are in the last interval of length $T_{\min}$ at the moment of the arrival of inhibition will be synchronized, due to the 'river picture', and will spike after approximately $T_{\min}$, giving rise to the first cluster. During this period, the cells in the second last interval of length $T_{\min}$ will continue to the last interval of length $T_{\min}$, without feeling much inhibition. When the second volley of inhibition arrives, these cells form a cluster, etc. Now suppose that the interval $[0, T_{\max}]$ can be covered by $k - 1$ copies of interval of length $T_{\min}$ plus a remaining interval of length smaller than $T_{\min}$ (except for special cases). By the argument above, the number of clusters should be given by k.

Expressing this by a formula, we have the following estimate for the existence of a solutions with k clusters:

$$(k-1)T_{\min} + k(\delta_E + \delta_I) < T_{\max}. \tag{6}$$

(recall that δ_E (resp. δ_I) are the delay of the arrival of excitation (inhibition)). Note that the maximal number of clusters corresponds to the largest k satisfying (6), but solutions with fewer clusters are not excluded. We define:

$$k_{\max} = \frac{T_{\max} - \delta_E - \delta_I}{T_{\min} + (\delta_E + \delta_I)} + 1. \tag{7}$$

Inequality (6) is now equivalent to $k < k_{\max}$.

We have done a number of simulations and compared them with the predictions of Eq. (6). In most simulations the estimate is too low, but we have found some situations when it is too high. We found that for many parameter values there exist multiple clustered states. We can obtain some of them by using nearby initial conditions for which a similar

cluster state exists. Other solutions are obtained from a *phase distributed initial condition*, obtained by taking a solution of a single MT cell, with the natural time parametrization (which we often refer to as phase), and translating the time variable by small intervals to obtain initial conditions for different cells in Eq. (2).

As mentioned, for solutions obtained from nearby initial conditions (6) typically underestimates the maximal number of clusters. A possible explanation for this is that the slope of the TTS function is very close to 0 only for a very small range of the natural time variable of the MT cell, which increases the possibility of small clusters. To see this imagine a group of E-cells loosely arranged in a cluster. Suppose the leading cells spike, causing a volley of inhibition. If inhibition arrives soon enough then the cells that were behind are stopped from spiking– this leads to two or more

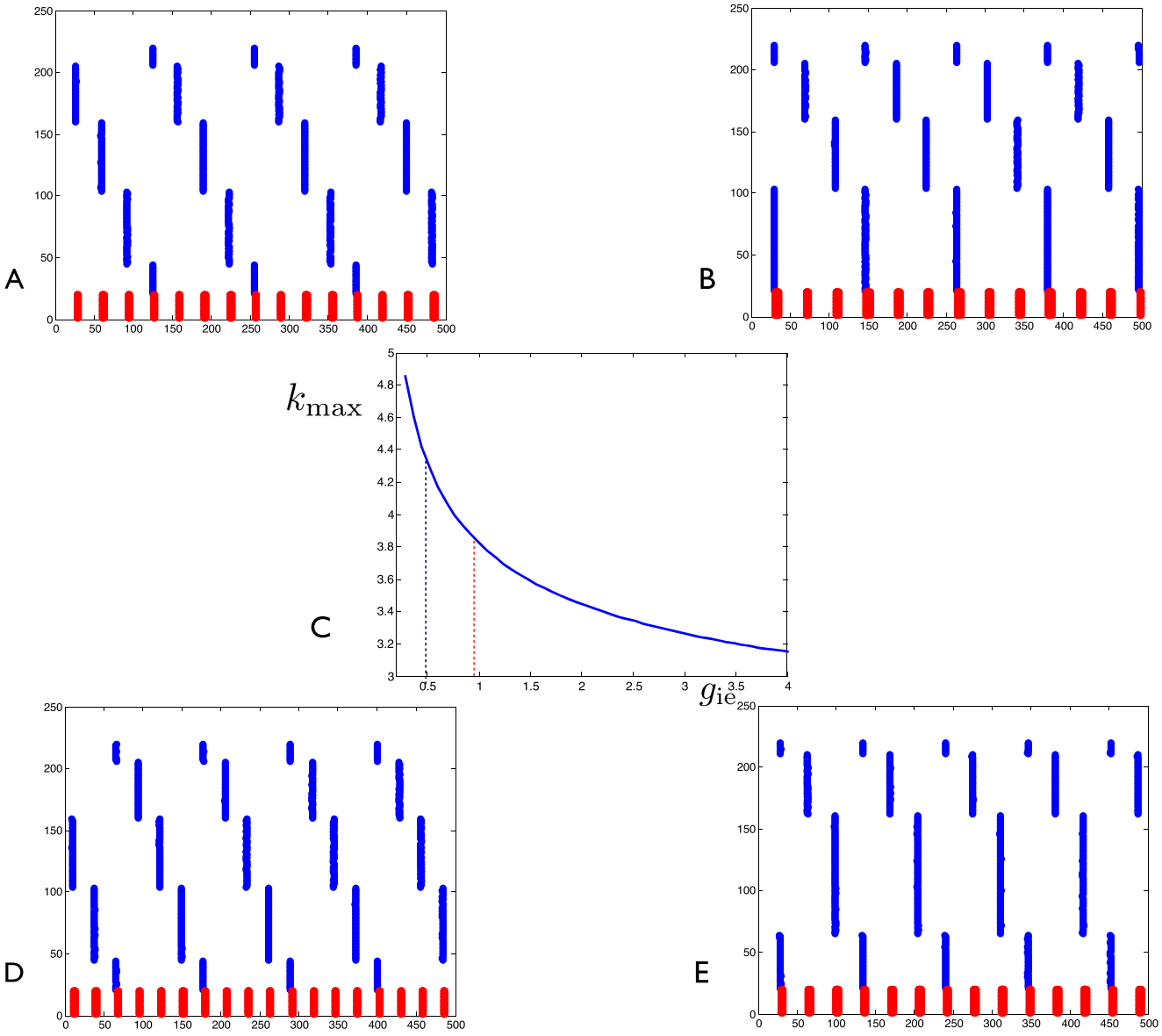

Fig. 7 The prediction of Eq. (6) was compared to the value of g_{ie} for which the change in the number of clusters actually occurs. The solutions in panels A and B were computed from an initial condition given by an existing clustered solution for a lower value of g_{ie}. *Dashed red line* in panel C marks the transition from four to three clusters for this type of solutions. For this choice of parameters (6) gives a pretty close, but too low estimate of the number of clusters. The solutions in panels D and E were computed from a phase distributed initial condition, same for all parameter values. Dashed black line in panel C marks the transition from four to three clusters for this type of solutions. For this choice of parameters (6) gives an overestimate of the number of clusters. **A** A four cluster solution for $g_{\mathrm{AHP}} = 2.3$, $I = 4$ and $g_{ie} = 0.9$. **B** A three cluster solution for for $g_{\mathrm{AHP}} = 2.3$, $I = 4$ and $g_{ie} = 1$. **C** The expression $k_{\max}$, defined by Eq. (7), computed as a function of g_{ie}, with $T_{\max}$ and $T_{\min}$ evaluated numerically

separate clusters. If inhibition comes later then all the cells in the loosely organized cluster can spike before it arrives – in this case just one cluster is formed. By varying parameters to increase the delay between the spikes of the E cells and the arrival of inhibition (e.g. increasing δ_I) one can improve the accuracy of Eq. (6). In Fig. 7 we show a plot of $k_{\max}$ (panel C). This plot predicts a change from four to three clusters at $g_{ie} \approx 0.8$, however simulations show that for solutions obtained from nearby initial conditions the change actually occurs for $g_{ie} \approx 1$. The estimate given (6) is close, but too low. To obtain Fig. 8 we decreased δ_I. The number of clusters is now significantly larger than predicted by Eq. (6). For this simulation the effect of varying g_{ie} is more pronounced, i.e. as g_{ie} is varied there are more possibilities for clustered solutions. Summarizing, the larger the delay of the arrival of inhibition after a spike of E-cells, the more accurate the formula. On the other hand the effect of changing g_{ie} on the maximal number of clusters becomes stronger when the delay of the arrival of inhibition is smaller.

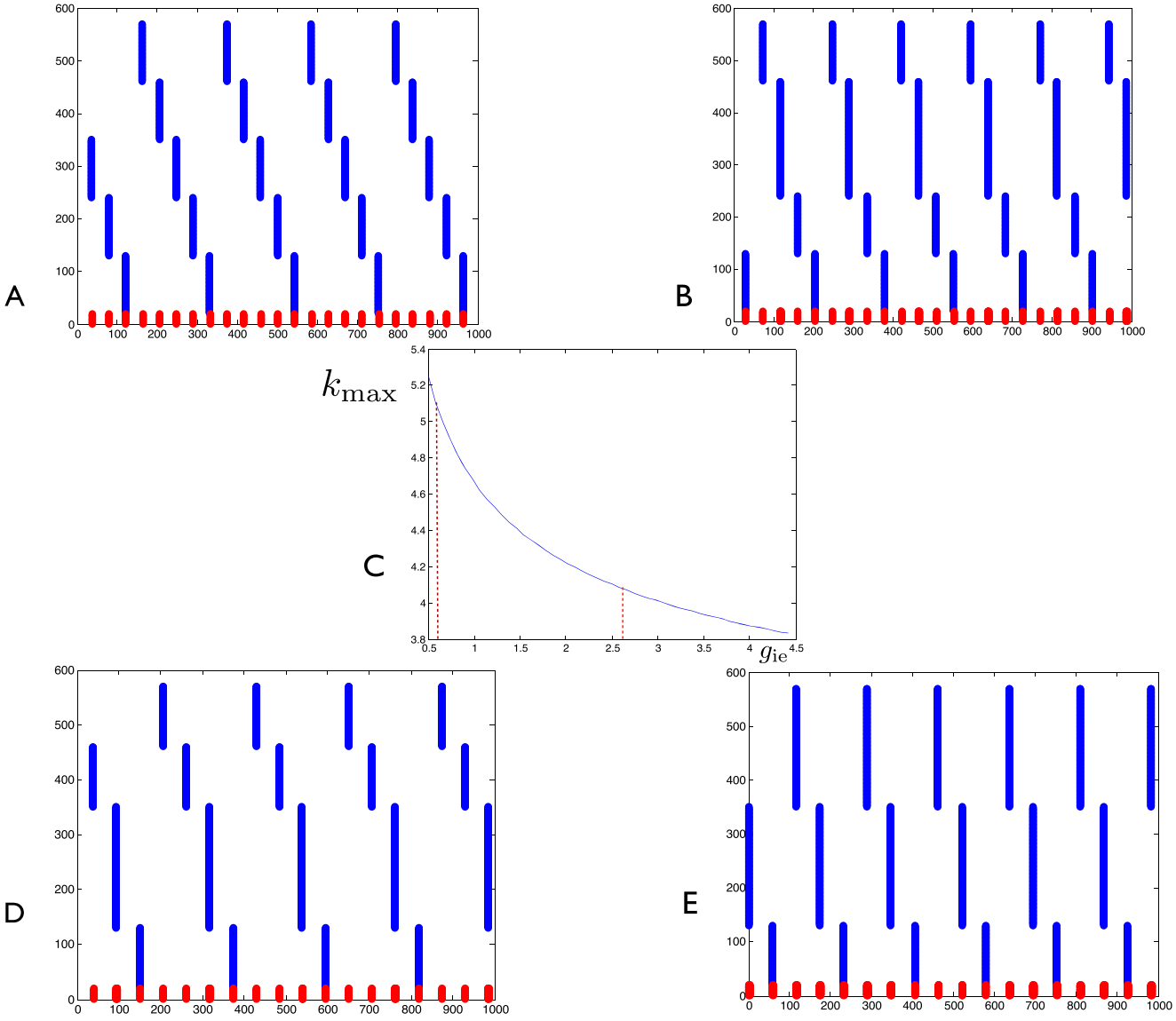

Fig. 8 In this simulation we decreased the value $\delta_E + \delta_I$ as well the drive to the I cells I_i. We used $\delta_E = \delta_I = 0.1$ and $I_i = 0.5$ as opposed to $\delta_E = 0.1$, $\delta_I = 0.2$ and $I_i = 0.52$, used in the simulations shown in Fig. 7. All solutions were computed from initial conditions given by a clustered solution existing for a nearby parameter setting. Changing the parameters resulted in the occurrence of more clusters and in the reduction of the accuracy of Eq. (6). **A** A five cluster solution for $g_{\text{AHP}} = 2.3$, $I = 4$ and $g_{ie} = 0.8$. **B** A four cluster solution for $g_{\text{AHP}} = 2.3$, $I = 4$ and $g_{ie} = 0.9$. **C** The expression $k_{\max}$ computed as a function of g_{ie}, with $T_{\max}$ and $T_{\min}$ evaluated numerically. The changes from a five cluster to four cluster and from a four cluster to three clusters are marked by red lines. **D** A four cluster solution for $g_{\text{AHP}} = 2.3$, $I = 4$ and $g_{ie} = 1.7$. **E** A three cluster solution for $g_{\text{AHP}} = 2.3$, $I = 4$ and $g_{ie} = 1.8$

For solutions obtained from phase distributed initial conditions (6) typically overestimates the maximal number of clusters, see Fig. 7, panels D and E. One possible explanation is that the assumption of a rapid change of the slope of the TTS function from near 0 to near -1 is not accurate. In fact the slope of the TTS function increases fairly gradually (see Fig. 6), so that even cells that are far away from spiking are still affected by inhibition. This is due to the fact that inhibition, no matter in which stage of the cycle, adds to the leakiness of the cell, and hence increases the value of the TTS function. Hence inhibition is effective over a larger range of the phase variable (natural time variable of the MT cell) than given by $T_{\min}$.

The arguments presented in this section are heuristic as we are not able to obtain rigorous results in the context of Eq. (2). In Section 3.2, where we study phase PING, i.e. system (3), we obtain more rigorous results. In particular we derive asymptotic estimates for $T_{\min}$ and $T_{\max}$, which, in combination with Eq. (6) gives an estimate of the number of clusters as a function of the key parameters of the model. This estimate depends not just on the parameters of the adaptation current, but also on inhibition. Using a limit obtained by letting adaptation and inhibition simultaneously increase towards ∞ in such a way that the number of clusters predicted by Eq. (6) is constant, we prove that Eq. (6) gives a sharp estimate, see Theorem 1 for a precise statement.

3.2 Phase PING

Phase PING (see Section 2.3, system (3)) is a toy model in which we have replaced the MT cells with phase oscillators and introduced the coupling function $\theta \mapsto f((\theta - \theta_{\text{left}})/\omega)$, where θ_{left} is given by Eq. (4), T_0 is a fixed constant, $f(t) = 0$ for $t \notin (0, T_0)$ and is quadratic on $(0, T_0)$ (with value $T_0 = 20$). An accurate computation of the PRC was carried out in Kilpatrick and Ermentrout (2011). The choice of the coupling function (PRC) which we made here is motivated by the wish to simplify the arguments. Our results could, however, be extendend to the case of a more accurate PRC. Finally, note that the parameter ω in Eq. (3) plays a similar role as g_{AHP} for Eq. (2).

For this model it is possible to get good analytic estimates for $T_{\max}$ and $T_{\min}$. We will also determine when and with what rate the phases representing different cells approach each other. Finally, in a limit consisting of simultaneously letting $\omega \to 0$ and $g \to \infty$ in such a way that the number of clusters predicted by Eq. (6) remains constant, we prove that Eq. (6) is an optimal estimate, i.e. there exists a stable periodic solution with k clusters, with k maximal given by Eq. (6) and there is no such solution with more than k clusters. In this section we have focused on the two parameters ω and g, and on the dependence of the two derived quantities $T_{\min}$ and $T_{\max}$ on these parameters.

As our arguments are based on the 'river picture' of Börgers and Kopell (2003), we begin by reviewing this approach in the context of Eq. (3).

3.2.1 Review of the 'river picture' of Börgers and Kopell (2003)

Börgers and Kopell (2003) consider a PING model with both E-cells and I-cells given by theta neurons. They study the existence of oscillations in which all the E-cells as well as all the I-cells fire in synchrony (with slight delay between the E-cells and the I-cells). In the simplest case they assume that the E-cells are not coupled to each other, so that each E-cell can be considered independently, i.e. as a single cell receiving a volley of inhibition. Before we go on let us point out two differences between our approach. First, we use phase oscillators, rather than theta neurons, which, we feel, simplifies the presentation, although, as shown by Kilpatrick and Ermentrout (2011), theta neurons can also be used, leading to analytic solutions. Reduction to phase oscillators can be made in a rather general context (Ermentrout and Kopell 1991), which means that the applicability of our approach is quite general. The second difference is that, rather than using the concept of 'river', we use Fenichel slow manifold (Fenichel 1979). These two concepts have a similar meaning, however 'river' was introduced using non-standard analysis, so that its precise meaning is not accessible to the authors of this paper.

For $\omega = 1/T_0$ system (3) has properties analogous to those of the model studied by Börgers and Kopell (2003). In this case $\theta_{\text{left}} = 0$, so that the coupling function (PRC) is non-zero on the entire interval $[0, 1]$. Following the footsteps of Börgers and Kopell (2003) we study the dynamics of a single E-cell in the presence of inhibition. In the context of Eq. (3) with $\omega = 1/T_0$ this equation is given by

$$\begin{aligned} \frac{d\theta}{dt} &= \omega - gsf(\theta/\omega) \\ \frac{ds}{dt} &= -\varepsilon s; \qquad\qquad s(0) = 1. \end{aligned} \tag{8}$$

Recall that f has a parabolic shape with maximal value f_M. We will assume that inhibition is sufficiently strong, i.e. the condition

$$\omega < gf_M \tag{9}$$

is satisfied. System (8) is slow/fast and all solutions starting with $s = 1$ and arbitrary θ are exponentially attracted to a Fenichel slow manifold, which is one dimensional, locally

invariant, and, in this case, parametrized by a solution. The phase portrait of Eq. (8) is given in Fig. 9. The idea is now that all solutions, with initial conditions corresponding to the states of different E-cells at the time of the arrival of inhibition, are strongly attracted to each other, i.e. their θ components quickly approach each other (the s components are already equal). The Fenichel slow manifold can be thought of as a river attracting all the nearby solutions. Any two solutions are extremely close to each other at the time when they reach the vicinity of the critical point of f, thus the cells they represent spike almost at the same time.

We end this section on few remarks concerning the use of singular perturbation theory. The fact that ε is the inverse of the time constant of inhibition, which equals approximately 9 ms, may cast a doubt on the relevance of singular perturbation theory. Another point is that the inverse of the time constant of adaptation is a much smaller parameter (used by Kilpatrick and Ermentrout (2011) in their perturbation analysis). We feel that our approach is an interesting alternative, for the following reasons. First, the hallmark feature of singular perturbation theory is the presence of strong contraction and the synchronization brought about by inhibition (river picture) is precisely that. Second, even though singular perturbation only works, mathematically, in the limit of $\varepsilon \to 0$, its predictions often extend to ε not so close to 0. The reason for this is that strong contraction/expansion can be present even when ε is not so small. For example, $\varepsilon = 0.1$ may give (positive or negative) eigenvalues of the order of e^{10}. Simulations of the toy model with $\varepsilon = 0.1$ (see Figs. 11 and 10) were in reasonable agreement with the singular perturbation estimates.

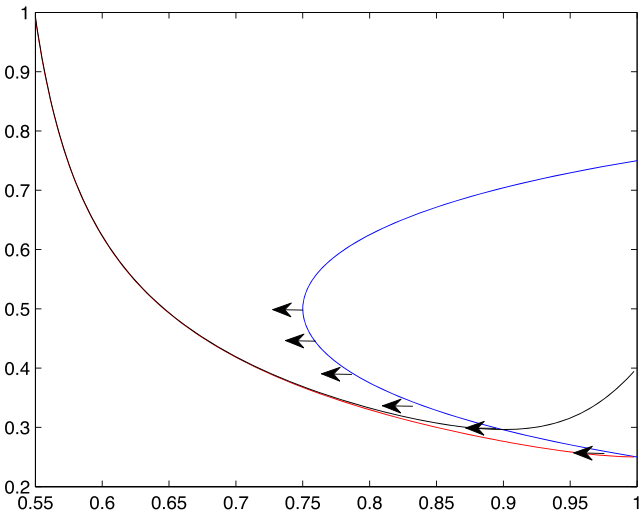

Fig. 9 The 'river effect'. The curve of quasi stationary points (*blue*) and two solutions (*black* and *red*)

3.2.2 Extension of the 'river picture'

We now consider the general case of $\omega \ll 1/T_0$. The system corresponding to an E-cell subjected to a spike of inhibition (generalization of Eq. (8) now has the form:

$$\begin{aligned} \frac{d\theta}{dt} &= \omega - gsf((\theta - \theta_{\text{left}})/\omega) \\ \frac{ds}{dt} &= -\varepsilon s; \qquad\qquad s(0) = 1, \end{aligned} \tag{10}$$

where f is as defined in Section 2.3, i.e. f is quadratic on the interval $(0, T_0)$, and 0 otherwise. For Eq. (10) the picture is more complicated than for Eq. (8). We distinguish three cases:

$\theta_{\text{left}} < \theta < 1$ Here the 'river picture' fully applies, so that any two cells with initial condition satisfying this condition are attracted to each other and fire almost instantenously.

$1 - \omega T_{\min} < \theta$ As mentioned earlier, due to inhibition, there exists a minimal time needed for any initial condition (10) to reach a spike. We denote this time by $T_{\min}$. Solutions satisfying $1 - \omega T_{\min} < \theta$ experience a delay to spike and there is some contraction between any two solutions starting in this region. In the sequel we will show that, in the aforementioned limit of ω approaching 0 with g adjusted simultaneously so that $\omega(T_{\min} + \omega\delta)$ stays fixed, trajectories starting in this region can be attracted to each other to form a a cluster.

$\theta < 1 - \omega T_{\min}$ Solutions starting at θ are not affected by inhibition and therefore spike at approximately the same time as they would have if inhibition had not been present. Given solutions with initial conditions θ_1 and θ_2, with θ_1 or θ_2 satisfying $\theta < 1 - \omega T_{\min}$, the corresponding solutions are not attracted to each other.

The TTS function is determined by the solutions of Eq. (10) and assigns to every θ_0 the time needed for the solution of Eq. (10) with $\theta(0) = \theta_0$ to reach the firing threshold $\theta = 1$.

3.2.3 Computation of T_{min} and the contraction rate

Let

$$s_M = \frac{\omega}{gf_M}. \tag{11}$$

By Eq. (9) $s_M < 1$.

To fix ideas we use a specific definition for f, namely:

$$f(t) = \frac{4t(t - T_0)}{T_0^2}. \tag{12}$$

We will argue that the approximate value of $T_{\min}$ is:

$$T_{min} \approx -\frac{1}{\varepsilon} ln(s_M) - \Omega_0 \left(\frac{T_0^2}{4\varepsilon}\right)^{1/3} \tag{13}$$

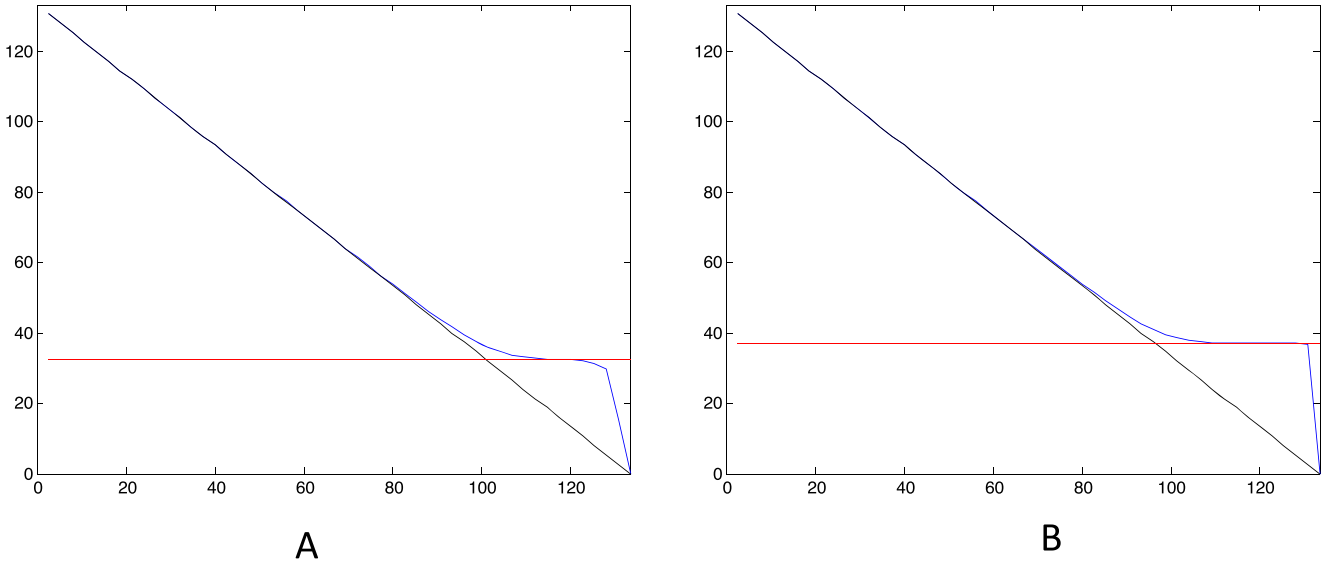

Fig. 10 The TTS function for phase PING shows the validity of the approximation of T_{min} by Eq. (13) for $\omega = 0.0075$ and $\varepsilon = 0.1$. The *red horizontal line* corresponds to the value of T_{min} as predicted by Eq. (13) with $g_{ie} = 0.3$ in panel **A** and $g_{ie} = 0.5$ in panel **B**

where $\Omega_0 \approx -2.34$ is a universal constant whose meaning will be explained in the Appendix.

Figure 10 shows examples of the application of Eq. (13).

We will now show how Eq. (10) can be transformed to a slow/fast system for which estimate (13) can be obtained from existing results. We first rewrite Eq. (13) as a sum of two terms

$$T_{\text{min}} = T_{\text{SN}} + T_{\text{esc}} \quad T_{\text{SN}} = -\frac{1}{\varepsilon} ln(s_M),$$
$$T_{\text{esc}} = -\Omega_0 \left(\frac{T_0^2}{4\varepsilon}\right)^{1/3}$$

The time T_{SN} is defined as the time needed for s to decrease from 1 to s_M. If s is treated as a constant ($\varepsilon = 0$ limit in Eq. (10)) then s_M is a point of saddle-node bifurcation. For $\varepsilon > 0$, while $s > s_M$, there is an attracting Fenichel slow manifold close to the curve $(s, \theta(s))$, where $\theta(s)$ is a solution of

$$0 = \omega - gsf((\theta - \theta_{\text{left}})/\omega),$$

and every other solution has to follow the slow manifold. This implies that the time it needs to reach the vicinity of f_M is approximately $\log(1/s_M)$.

To get the estimate of T_{esc} we begin by a transformation:

$$x = \frac{\theta - \theta_{\text{left}}}{\omega}, \quad s = s_M \tilde{s}.$$

In the new coordinates Eq. (10) becomes

$$\frac{dx}{dt} = 1 - \tilde{s} f(x)$$
$$\frac{d\tilde{s}}{dt} = -\varepsilon \tilde{s}; \qquad \tilde{s}(0) = 1. \tag{14}$$

Note that the term gsf_M/ω is less than 1 for $s > s_M$. We replacing x by $\tilde{x} + 1$ and Taylor expand at $(\tilde{x}, \tilde{s}) = (0, 1)$, which, at lowest order, gives the followng system:

$$\frac{d\tilde{x}}{dt} = (1 - \tilde{s}) - B\tilde{x}^2$$
$$\frac{ds}{dt} = -\varepsilon, \tag{15}$$

where $B = 4/T_0^2$. Based on a result of Krupa and Szmolyan (2001) (a review of this result with precise references will be given in the Appendix) we can give an estimate

$$T_{\text{esc}} = -\Omega_0 (B\varepsilon)^{1/3} = -\Omega_0 \left(\frac{T_0^2}{4\varepsilon}\right)^{1/3} \tag{16}$$

3.2.4 Estimate of T_{max}

The value of T_{max} equals the time it takes for a solution of Eq. (10) with $\theta(0) = 0$ to reach $\theta = 1$. Note that $T_{max} > 1/\omega$, but when ω is sufficiently small then the following holds. If the inhibition comes at the beginning of the cycle it decays to negligible size by the time the phase advances to the regime where inhibition could have an effect. Hence, in this case

$$T_{max} \approx \frac{1}{\omega}. \tag{17}$$

For ω larger T_{max} can be significantly larger than $1/\omega$, but the maximal value it can reach is

$$T_{max} \approx \frac{1}{\omega} + T_{min}. \tag{18}$$

Also, a rise in g_{ie} could lead to a loss of accuracy of Eq. (18).

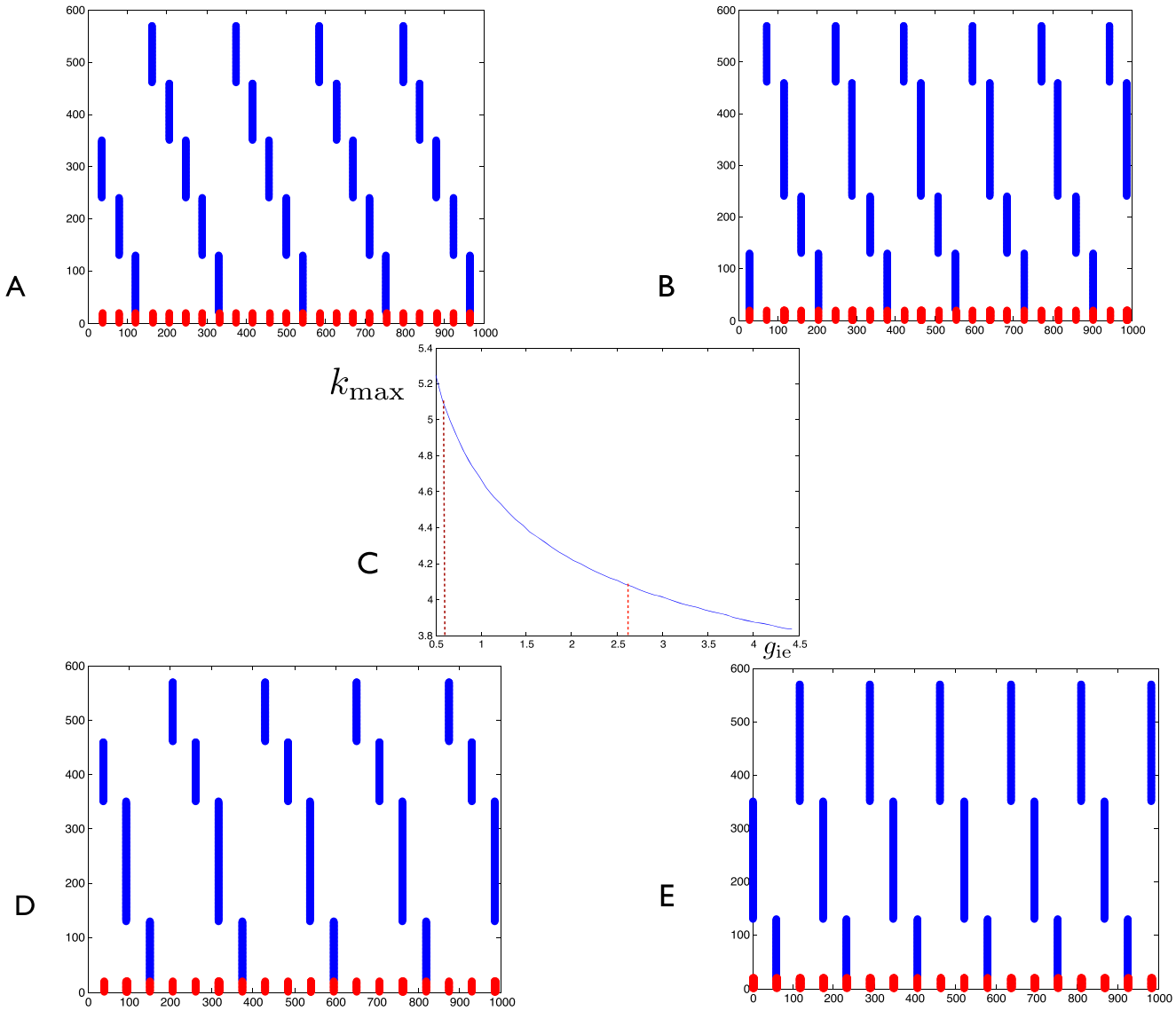

Fig. 11 Changes in the number of clusters as a function of g_{ie} and the estimate Eq. (19). All solutions were computed from initial conditions given by a clustered solution existing for a nearby parameter setting. **A** A 5-cluster solution for $\omega = 0.006$, $g_{ie} = 0.58$, $\varepsilon = 0.1$. **B** A 4-cluster solution for $\omega = 0.006$, $g_{ie} = 0.59$, $\varepsilon = 0.1$. **C** Graph of $k_{\max}$ (defined by Eq. (29)) as a function of g_{ie} with transitions between regimes of different numbers of clusters marked by *dashed red lines*. **D** A 4-cluster solution for $\omega = 0.006$, $g_{ie} = 2.52$, $\varepsilon = 0.1$. **E** A 3-cluster solution for $\omega = 0.006$, $g_{ie} = 2.53$, $\varepsilon = 0.1$

3.2.5 Existence and stability of clustered solutions

Recall condition Eq. (6) which gave an estimate for the maximal number of clusters. Combining Eqs. (6), (13) and (17) we derive an explicit estimate for the toy model:

$$(k-1)(T_{\min} + \delta_E + \delta_I) < 1/\omega - (\delta_E + \delta_I), \tag{19}$$

where $T_{\min}$ is given by Eq. (13). Note that Eq. (19) depends in a very significant way on ω, but it also depends on the maximal conductance of inhibition g_{ie} and on the decay time constant of inhibition τ. There are many reasons why Eq.(19) would give a too high estimate. One such reason is that clusters should be sufficiently large to cause a spike of the I cells. The estimate can also be too low if Eq. (17) is not accurate. The strength of inhibition may also have an influence on the stability of clustered solutions. Inhibition has the effect of bringing together the cells in each cluster. In other words, sufficient inhibition is necessary for stability of clustered solutions (see Eq. (23)). Hence if g_{ie} is too small, the rhythm may be unstable.

In the sequel of this section we consider the limit of ω going to 0 with g simultaneously adjusted to keep the quantity $\omega(T_{\min} + \delta_E + \delta_I)$ constant. Heuristically, this means that we keep the number of clusters constant but increase

the strength of inhibition and thus the strength of the 'river effect'.

The phase space of Eq. (3) is given by points of the form $(\theta_1, \ldots, \theta_N, w_1, \ldots, w_M)$, where N is the number of E-cells and M the number of I-cells (for simplicity of notation we suppress the dependence of phase points on synaptic variables). In this work we assume that the I-cells are in the excitable regime but very close to the firing threshold so that they fire as soon as the spike from the E-cells arrives. We will also assume that there is no delay of the arrival of the inhibition to the E-cells ($\delta_I = 0$). On the other hand we will keep the delay of the arrival of excitation as positive. This is necessary to ensure that the E-cells that are very close can form clusters (the cell slightly behind can spike without being stopped by inhibition). To simplify the notation we will write $\delta = \delta_E > 0$. We also only consider the value of k which is maximal to satisfy Eq. (19). With these convention we re-write Eq. (19) to obtain

$$\omega\delta < 1 - (k-1)\omega(T_{\min} + \delta)) < \omega(T_{\min} + \delta) + \omega\delta. \quad (20)$$

We define $\theta_{\min} = \omega(T_{\min} + \delta)$ and re-write Eq. (20) in the form:

$$\omega\delta < 1 - (k-1)\theta_{\min} < \theta_{\min} + \omega\delta. \quad (21)$$

Note that for fixed $\theta_{\min}$ and ω estimate (21) defines a unique k, except for the cases when one of the inequalities becomes an equality for some integer k.

We now introduce the subset C_k of the phase space corresponding to k-cluster states. Elements of C_k are defined as follows: for each $p = (\theta_1, \theta_2, \ldots \theta_N, w_1, \ldots w_M) \in C_k$ there exist $\theta_1^c, \ldots \theta_k^c$, and indices $1 = j_1 < j_2 < \ldots < j_k < j_{k+1} = N$ such that $\theta_j = \theta_l^c$ for $j_l \le l < j_{l+1}$. Note that $j_{l+1} - j_l$ gives the number of elements in cluster j and θ_l is the common value of θ corresponding to each cluster. Thus defined clusters are ordered but for non-ordered clustered one could apply the same arguments by re-numbering the equations.

Theorem 1 *Let k be an integer satisfying (21). Then, provided that ω is sufficiently small and g is adjusted so that θ_{min} stays constant, system (2) has a stable k-cluster periodic solution and does not have a periodic solution with more than k clusters.*

Proof We define sections Σ_j by the condition $\theta_j = \omega\delta$ (the jth neuron is at time δ after its reset value, which corresponds to the moment of the arrival of inhibition). We will search for cluster states as fixed points of the return map from Σ_1 to itself. By definition, points in Σ_1 have the form $(\omega\delta, \theta_2, \ldots \theta_N, w_1, \ldots, w_M)$, points in Σ_2 have the form $(\theta_1, \omega\delta, \ldots \theta_N, w_1, \ldots, w_M)$, etc. We consider firing maps $\pi_{j,l}^f$ mapping Σ_j to Σ_l; these maps are defined for states in Σ_j for which cell l will be the first one to fire, with the image given by the solution at $t = \delta$ after the spike of the l-th cell. We look for cluster states obtained by application of composition of firing maps corresponding to different clusters. For an initial condition in $\Sigma_1 \cap C_k$ we assume that the k-th cluster fires first, then cluster $k-1$, and so on, in decreasing order. An argument for firing events occurring in in a different order is similar and will be omitted. We identify elements of C_k with the sequences $(\theta_1^c, ..., \theta_k^c)$ and $(j_1, \ldots, j_{k+1})$. We define firing maps π_l^f as π_{j_{l+1}, j_l}^f ($N+1 \equiv 1$ and $k+1 \equiv 1$), i.e. cluster $l-1$ fires after cluster l.

Let $p_l = (\theta_1^{c,l}, \ldots, \theta_m^{c,l})$, $m \ge k$ be a sequence of cluster states corresponding to a fixed point of the return map, i.e. $p_2 = \pi_k^f(p_1)$, $p_3 = \pi_{k-1}^f(p_2)$, ..., $p_m = \pi_2^f(p_{m-1})$ and $p_1 = \pi_2^f(p_m)$. Note that $\theta_1^{c,j} \ge \omega\delta + j\omega(T_{min} + \delta)$, since the time between consecutive firings is at least $T_{\min} + \delta$. By Eq. (20) cluster 1 must be the one to fire next, see Proposition 1. Hence a cluster with more than k states cannot exist.

We now prove that Eq. (20) is sufficient for the existence of k clusters. We consider the sequence $(\theta_1^c, \ldots, \theta_k^c)$ satisfying $\theta_j^c = \omega\delta + (j-1)\theta_{\min}$, $j = 1, \ldots, k-1$, and consider a state p with k clusters (approximately the same size) defined by this sequence, with $w_1 = w_2 = \ldots w_M = w_e$, where w_e is the excitable equilibrium of the QIF model governing the dynamics of the I-cells. By Eq. (21), θ_k^c is the only one of the θ_j^c's to satisfy $1 - \theta_m in < \theta_k^c < 1$, hence the kth cluster will be the first one to fire. By Proposition 1 the spike will happen approximately at $t \approx T_{\min}$ and the time cluster k reaches section Σ_k will be $t \approx T_{\min} + \delta$. Let $p_2 = \pi_k^f(p) = (\theta_1^{c,2}, \ldots, \theta_{k-1}^{c,2}, \omega\delta)$. Clearly $\theta_{k-1}^{c,2} \approx \omega\delta + (k-1)\theta_{\min}$. By the same argument cluster $k-1$ fires next and we can construct the point $p_3 = \pi_{k-1}^f(p_2)$, etc., until we obtain p_k equal to the image of p by $\pi_1^f \pi_2^f \ldots \pi_k^f$ and very close to p. Let V be a small neighborhood of p in the phase space. If V is small enough than the return map restricted to V equals $\pi_1^f \pi_2^f \ldots \pi_k^f$, and is a contraction, by Proposition 2. Hence, by the contraction mapping theorem, a stable k-cluster state exists. □

Proposition 1 *Fix θ_* satisfying*

$$1 - \omega T_{min} < \theta_* < 1.$$

Suppose that ω converges to 0 with g increased simultaneously so that ωT_{min} stays fixed. Let T_* be the time needed for the solution of Eq. (10) with $\theta(0) = \theta_*$ to reach the firing threshold. Then T_* converges to T_{min} as ω approaches 0.

Proof Let $\theta(t)$ denote the solution of Eq. (10) with $\theta(0) = \theta_*$. Let

$$T_1 = \frac{1 - \theta_*}{\omega}.$$

If $T_1 < T_{\rm SN}$ then $s(T_1) > s_M$. In this case, by Proposition 2, the solution $\theta(t)$ will be attracted to the solution of Eq. (10) with initial condition $\theta_l = (1-\omega T_0)$ and will spike at $T \approx T_{\rm min}$. By definition of θ_* we have $(1-\theta_*) < \omega T_{\rm min}$. Since $T_{\rm esc}$ does not depend on ω and g, $\omega(T_{\rm SN} - T_{\rm min}) \to 0$ as ω approaches 0 with g adjusted so that $\omega T_{\rm min}$ stays fixed. It follows that, for ω sufficiently small $(1-\theta_*) < \omega T_{\rm SN}$. The result follows. □

Proposition 2 *Let $\theta_1(t)$ and $\theta_2(t)$ be two trajectories of Eq. (10) and suppose that there exists $0 < t_1 < T_{SN}$ with $\theta_l < \theta_j(t_1) < \theta_M$, $j = 1, 2$, where $\theta_l = 1 - \omega T_0$. Suppose that $s_1 = s(t_1) > s_M$ .The following estimate holds at the time of the spike:*

$$|\theta_1(t) - \theta_2(t)| \approx C|\theta_1(0) - \theta_2(0)| \tag{22}$$

where

$$C = e^{-\frac{1}{\varepsilon}\int_{s_M}^{s_1} f'((\theta_0(\sigma))/\omega - 1 + T_0)d\sigma}, \tag{23}$$

and $\theta_0(s)$ is the parametrization of the curve $\omega - sf(\theta) = 0$.

Proof By Fenichel theory (Fenichel 1979) there exists a slow manifold of Eq. (10) which is $O(\varepsilon)$ close to the curve $\omega - sf(\theta) = 0$. Such a slow manifold is sometimes called river, see Börgers and Kopell (2003). Let $\theta_{\varepsilon,0}$ be such that $(\theta_{\varepsilon,0}, 1)$ is on the slow manifold and let $(\theta_\varepsilon(t), s(t))$ be the solution of Eq. (10) satisfying $(\theta(t), s(t)) = (\theta_\varepsilon, 1)$. Note that $(\theta_\varepsilon(t), s(t))$ parametrizes the Fenichel slow manifold. The linearization of Eq. (10) is given as follows:

$$\begin{aligned} \frac{dv}{ds} &= -sf'(\theta_0(s))v \\ \frac{ds}{dt} &= -\varepsilon s; \qquad\qquad s(0) = 1; \end{aligned} \tag{24}$$

or

$$\frac{dv}{ds} = \frac{1}{\varepsilon} f'(\theta_\varepsilon(s))v \tag{25}$$

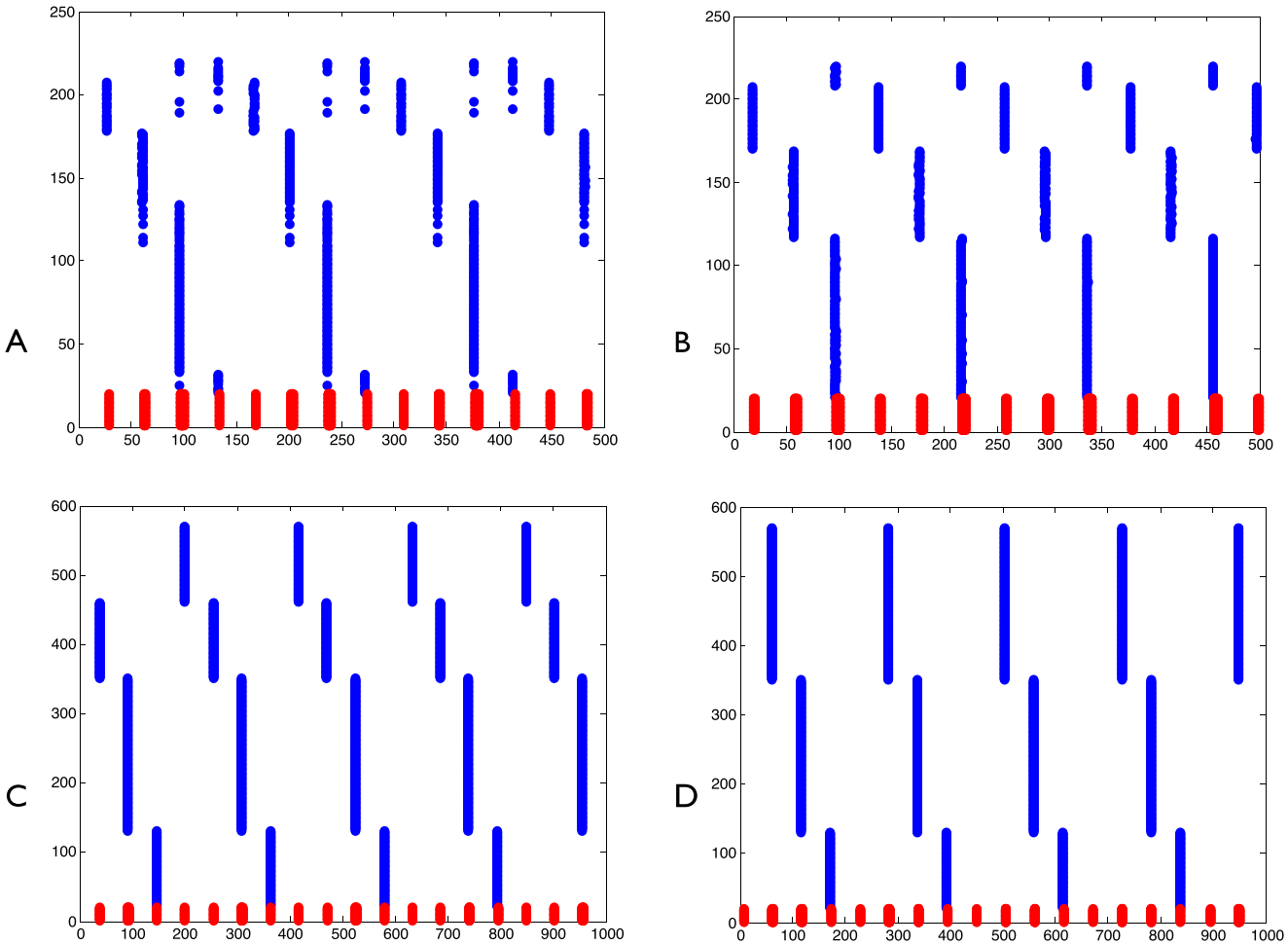

Fig. 12 Clustered solutions coexisting for the same parameter values **A** MT PING, solution with four clusters, existing for $I = 4$, $g_{AHP} = 2.3$ and $g_{ie} = 1.7$. **B** MT PING, solution with three clusters, existing for $I = 4$, $g_{AHP} = 2.3$ and $g_{ie} = 1.7$. **C** Phase PING, solution with four clusters, existing for $\omega = 0.006$, $g_{i.e.} = 2.1$. **D** Phase PING, solution with three clusters, existing for $\omega = 0.006$, $g_{i.e.} = 2.1$

We replace $\theta_\varepsilon(s)$ by $\theta_0(s)$, which is the the curve obtained by solving the equation $\omega - sf(\theta) = 0$ for θ as a function of s. We replace $\theta_\varepsilon(s)$ by $\theta_0(s)$ in Eq. (25), this incurs an error of $O(\varepsilon)$. We obtain

$$\frac{dv}{ds} = \frac{1}{\varepsilon} f'(\theta_0(s))v \tag{26}$$

A solution to Eq. (26) on an interval $[s_1, s_2]$ is given by

$$v(s) = v_0 e^{-\frac{1}{\varepsilon}\int_{s_1}^{s_2} f'(\theta_0(\sigma))d\sigma} \tag{27}$$

In other words the vector $v(s)$ contracts with the rate

$$C(s_1, s_2) = e^{-\frac{1}{\varepsilon}\int_{s_1}^{s_2} f'(\theta_0(\sigma))d\sigma}. \tag{28}$$

Now note that all the solutions of Eq. (10) starting in the interval $[\theta_l, 1]$, with $s < s_{\max}$ are attracted to the Fenichel slow manifold, hence any two such solutions have to attract each other with the rate given approximately by Eq. (28). □

In Fig. 11 we show a transition between the regimes of 5-cluster, 4-cluster and 3-cluster oscillations. Let

$$k_{\max} = \frac{1/\omega - (\delta_E + \delta_I)}{T_{\min} + \delta_E + \delta_I} + 1. \tag{29}$$

Clearly, the condition (19) is equivalent to $k < k_{\max}$. For the example shown in Fig. 11 the transition from five to four clusters occurs for $k_{\max} \approx 5.09$ and the transition from four to three clusters occurs for $k_{\max} \approx 4.09$. Hence, for these parameter values, the condition (19) gives a quite precise approximation of the maximal number of clusters.

3.2.6 Co-existence of cluster solutions and the effect of $E \to E$ connections

Estimate Eq. (6) does not exclude the existence of multiple stable cluster solutions. In fact there can exist solutions which have fewer clusters than given by the maximal k satisfying Eq. (6). Solutions with different number of clusters, co-existing for the same parameter values, are shown in Fig. 12 for both MT PING and phase PING.

The situation is even more complicated if $E \to E$ connections are included in the model ($g_{ee} > 0$). Figure 13, panel **A** shows a solution of the MT PING model in the presence of $E \to E$ connections and in the absence of inhibition ($g_{ie} = 0$) resulting from a simulation starting at a phase distributed initial condition. Clearly the E cells all spike at approximately the same time. If inhibition is 'turned on', i.e. the simulation is restarted with $g_{ie} > 0$, this solution remains stable, as inhibition arriving after the spike of the E-cells will have decayed before the E-cells return to the region where they can be affected by inhibition. However, if we perturb the synchronous state by adding a random perturbation then the resulting solution converges to a clustered state arising due to the action of the river mechanism as described at the end of Section 3.1.1 and in the proof of Theorem 1. Such a cluster solution is shown in Fig. 13, panel **B**.

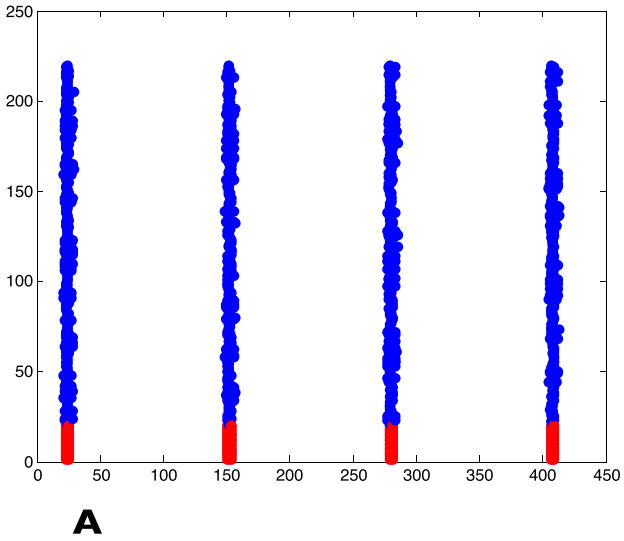

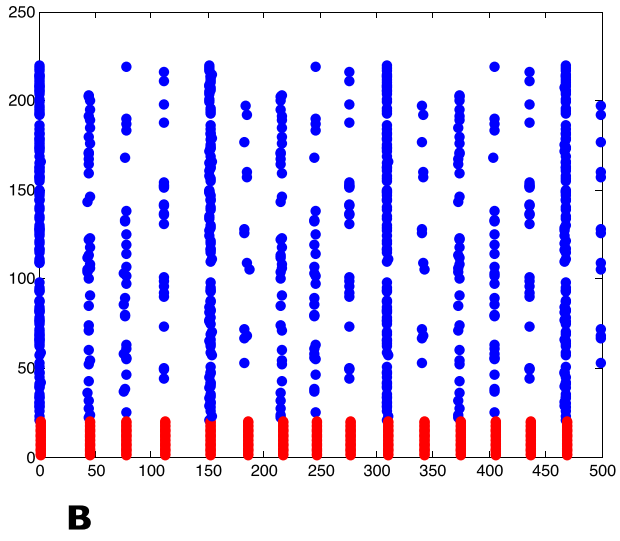

Fig. 13 E → E connections ($g_{ee} > 0$) provide a synchronization mechanism complementary to the river picture, enabling coexistence of stable solutions with full synchronization of E-cells and cluster solutions. **A** Solution of the MT PING model obtained for $g_{ee} = 0.3$ and $g_{ie} = 0$. The simulation was started at phase-distributed initial condition. **B** Four cluster solution of the MT PING model obtained for $g_{ee} = 0.3$ and $g_{ie} = 0.5$. The initial condition was obtained by a (sufficiently large) random perturbation of the solution shown in panel A. A synchronized solution still exists, (not shown) but has a small basin of attraction

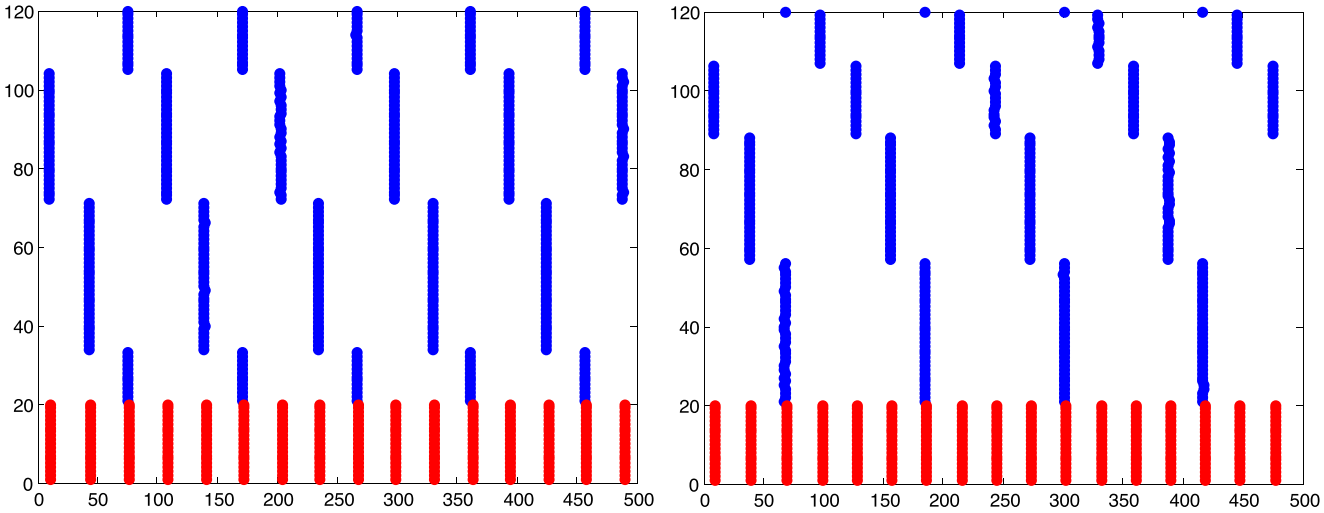

Fig. 14 Clustered solutions of the MT PING model with shunting inhibition, with $v_{rev} = -65$, $g_{ie} = 1.5$ and the drive to the E-cells $I = 1.1$. The left panel shows a solution with three clusters, corresponding $g_{AHP} = 0.35$ (maximal conductance of the AHP current) and the right panel shows a solution with four clusters, corresponding $g_{AHP} = 0.45$

3.3 Effects of shunting inhibition, MT PING

Since GABA-ergic inhibition can be shunting or partially depolarizing, with the reversal potential possibly close to or above the resting voltage of the cell, we have carried out simulations with $E_{GABA} = -65mV$. We expected that introducing shunting inhibition would reduce the interval of voltage values for which inhibition is effective, adding robustness to to the clustering effect, but the extent to which this was true was a surprise. Clustered solutions could be found at much lower values of g_{AHP} than for the hyperpolarizing case, see captions of Figs. 3 and 14. Moreover, oscillations with many clusters (four or five) could easily be found; thus the firing rate of individual pyramidal cells was less than 10 Hz for relatively small values of g_{AHP}. Rastergrams for rhythms with three and four clusters are shown in

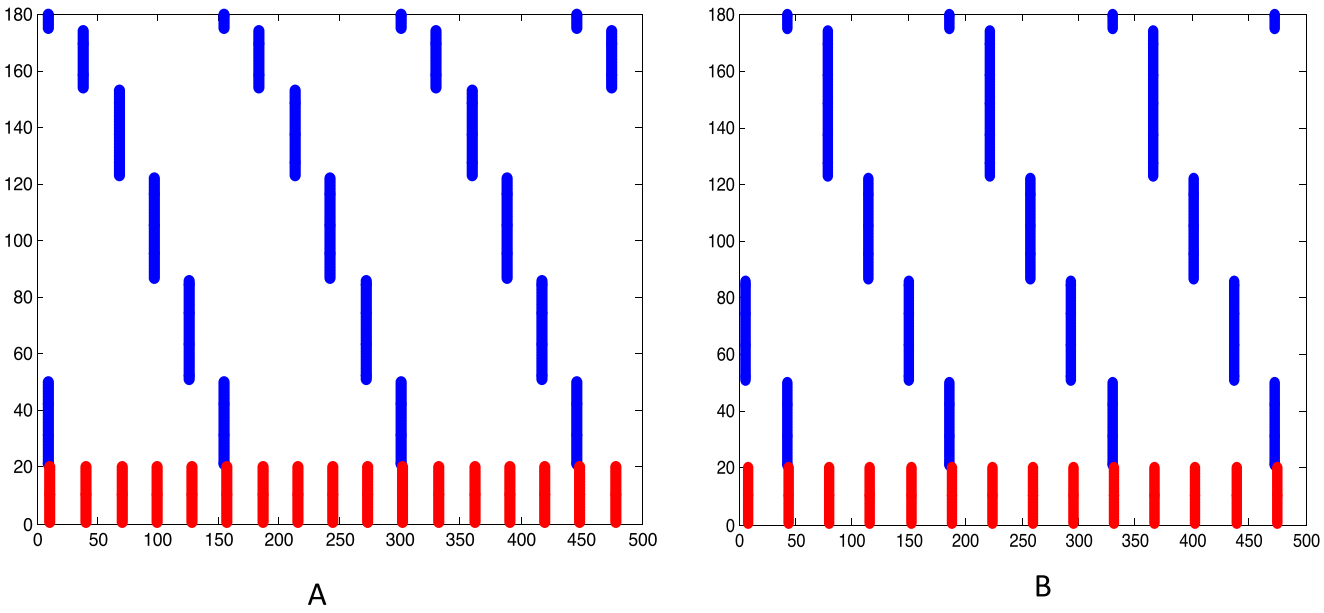

Fig. 15 Clustered solutions of the phase PING model with $\omega = 0.0075$, $g_{ie} = 0.3$, $\varepsilon = 0.1$. **A** Shunting inhibition. **B** Hyperpolarizing inhibition

Fig. 14. We note that the same strength of adaptation for the hyperpolarizing inhibition case leads to 0 clusters (global synchrony).

3.4 Effects of shunting inhibition, phase PING

Recall that to introduce the effect of shunting inhibition we modify the phase PING model by replacing the term $f((\theta_l - \theta_{\text{left}})/\omega)$ in the first equation of Eq. (3) with $f((\theta_l - \theta_{\text{left}})/\omega)\sigma(\theta)$, where σ is given by Eq. (5) (see end of Section 2.3 for the explanation of our modeling approach).

In Fig. 15 we show two oscillations, one for the phase model with shunting inhibition, as introduced above, and one for the original model. Note that ω is very low, yet in the case of shunting inhibition, an oscillation with fairly large gamma frequency is obtained.

4 Discussion

In this paper we have studied a PING model of gamma rhythm allowing for the existence of a rhythm with the excitatory (pyramidal) cells firing in clusters. We have shown how biophysical parameters, like the strength of the adaptation current, the strength of inhibition and the amount of external input can facilitate a transition between a rhythm where the pyramidal cells are synchronized and a clustered gamma, which we associate with weak gamma. Our work concerns the case of strong inhibition, as presented in Börgers and Kopell (2003). We have also shown that clustered gamma is more likely to arise if inhibition is shunting rather than hyperpolarizing.

In a recent study, Kilpatrick and Ermentrout (2011) also considered the clustered gamma oscillations, but concentrated mainly on the effect of the adaptation current. In our paper we obtain complementary results, exploring the effect that inhibition has on the formation on clusters and stability of clustered oscillations. We follow the approach of Börgers and Kopell (2003, 2005), using the fact that the time constant of inhibition is large as compared to the excitation. In addition, we rely on the assumption that the period of the pyramidal cell is very large, much larger than the time constant of inhibition. Thus there are three timescales in the system, with the ratio, approximately, 2:10:50. These assumptions form the basis of our perturbation analysis.

We focus on describing how the parameters of the system mediate the transitions between synchronous and clustered states. These parameters correspond to biophysical factors: the strength and the reversal potential of inhibition, the strength of the external input and the strength of the adaptation current. Various neuromodulators (as, for example acetylcholine, (Stiefel et al. 2009)) influence these parameters and could influence the type of gamma oscillation occurring at a particular moment. We know that adaptation currents are decreased by increasing the levels of acetylcholine (Stiefel et al. 2009). During bouts of increased cholinergic modulation one could expect seeing gamma with decreased number of clusters (increased synchronization). Other factors, like the cortical area where the oscillation is taking place, could also be a factor, since the cellular properties of pyramidal cells and interneurons as well as the synaptic properties could differ.

In this paper we considered a PING model with pyramidal cells being oscillators and interneurons being excitable. Complementary model of gamma oscillations is called ING, where the interneurons are oscillators. In the context of ING it is assumed that the drive feeds into the interneuron network and the projections from the pyramidal cells are negligible. Therefore an ING model consists only of interneurons. Bartos et al. (2007) showed that shunting inhibition plays an important role in stabilizing the synchronous oscillation, whereas Jeong and Gutkin (2007) suggested that for weak coupling shunting inhibition can promote clustering. It is an interesting question what happens to clustering in a population of pyramidal cells which receive input from such an interneuron network. As a follow-up of this work we intend to investigate clustered oscillations in such pyramidal cell networks.

Acknowledgments The research of MK was supported in part by a grant from the city of Paris (Bourse de la ville de Paris) and by CLS NWO grant to Stan Gielen. The research of BG was supported by the CNRS, INSERM, ANR, ENP, by Ville de Paris and by the Basic Research Program of the National Research University Higher School of Economics, Moscow, Russia. The research of SG was supported in part by the CLS program of NWO.

Conflict of interest The authors declare that they have no conflict of interest.

Appendix: Review of the result of Krupa and Szmolyan (2001) and the estimate of T_{esc}

Consider

$$\begin{aligned} \frac{dx}{dt} &= f(x, y) = -y + x^2 + O(xy, x^2) \\ \frac{dy}{dt} &= -\varepsilon(1 + O(x, y)). \end{aligned} \tag{30}$$

Note that system (30) has the same form as system (2.5) in Krupa and Szmolyan (2001). The following estimate is a consequence of Theorem 2.1 and Remark 2.11 in Krupa and Szmolyan (2001). Let Ω_0 be the smallest positive zero of the function

$$J_{-1/3}\left(\frac{2z^{2/3}}{3}\right) + J_{1/3}\left(\frac{2z^{2/3}}{3}\right),$$

where $J_{-1/3}$ (resp. $J_{1/3}$) are Bessel functions of the first kind.

Proposition 3 *Let $y_0 \geq 0$ and $x_0 < 0$ satisfy $f(x_0, y_0) = 0$. Also fix $\delta > 0$. Consider a family of solutions of Eq. (30) with initial conditions $x(0) = x_0 + O(\varepsilon)$ and $y(0) = y_0$. Let $(\delta, h(\varepsilon))$ be the intersection point of this trajectory with the line $x = \delta$. Then, for sufficiently small δ,*

$$h(\varepsilon) = \Omega_0 \varepsilon^{2/3} + O(\varepsilon \ln \varepsilon). \tag{31}$$

Now let T be the time needed for a trajectory with initial condition $x_0 < 0$, $y_0 = 0$. It follows from Eq. (31) and the form of Eq. (30) that $\varepsilon T \approx -\Omega_0 \varepsilon^{2/3}$. It follows that

$$T \approx -\Omega_0 \varepsilon^{-1/3}. \tag{32}$$

By scaling the variables and time (30) can be brought to the form Eq. (15) and estimate Eq. (16) can be obtained.

References

Bartos, M., Vida, I., Jonas, P. (2007). Synaptic mechanisms of synchronized gamma oscillations in inhibitory interneuron networks. *Nature Reviews Neuroscience, 8*, 45–56.

Börgers, C., & Kopell, N. (2003). Synchronization in networks of excitatory and inhibitory neurons with sparse, random connectivity. *Neural Computation, 15*(3), 509–539.

Börgers, C., & Kopell, N. (2005). Effects of noisy drive on rhythms in networks of excitatory and inhibitory neurons. *Neural Computation, 17*(3), 557–608.

Börgers, C., Epstein, S., Kopell, N. (2005). Background gamma rhythmicity and attention in cortical local circuits: a computational study. *Proceedings of the National Academy of Science USA, 102*(19), 7002–7007.

Cunningham, M.O., Whittington, M.A., Bibbig, A., Roopun, A., LeBeau, F.E.N., Vogt, A., Monyer, H., Buhl, E.H., Traub, R. (2004). A role for fast rhythmic bursting neurons in cortical gamma oscillations *in vitro*. *Proceedings of the Natural Academy of Sciences USA, 101*, 7152–7157.

Engel, A., Fries, P., Singer, W. (2001). Dynamic predictions: oscillations and synchrony in top-down processing. *Nature Reviews Neuroscience, 2*, 704–716.

Ermentrout, G.B., Pascal, M., Gutkin, B.S. (2001). The effects of spike frequency adaptation and negative feedback on the synchronization of neural oscillators. *Neural Computation, 13*, 1285–1310.

Ermentrout, G.B., & Kopell, N. (1991). *Journal of Mathematical Biology, 29*, 195–217.

Ermentrout, G.B., & Kopell, N. (1990). Oscillator death in systems of coupled neural oscillators. *SIAM Journal on Applied Mathematics, 50*(1), 125–146.

Fenichel, N. (1979). Geometric singular perturbation theory for ordinary differential equations. *Journal Differential Equations, 31*, 53–98.

Fries, P., Reynolds, J., Rorie, A., Desimone, R. (2001). Modulation of oscillatory neuronal synchronization by selective visual attention. *Science, 291*, 1560–1563.

Golomb, D., & Rinzel, J. (1994). Clustering in globally coupled inhibitory neurons. *Physica D, 72*, 259–282.

Gray, C.M. (1999). The temporal correlation hypothesis of visual feature integration: still alive and well. *Neuron, 24*, 31–47.

Jeong, H.Y., & Gutkin, B.S. (2007). Synchrony of neuronal oscillations controlled by GABAergic reversal potentials. *Neural Computation, 19*(3), 706–729.

Gutkin, B.S., Ermentrout, G.B., Reyes, A. (2005). Phase-response curves give the responses of neurons to transient inputs. *Journal of Neurophysiology, 94*, 1623–1635.

Jia, X., Smith, M.A., Kohn, A. (2011). Stimulus selectivity and spatial coherence of gamma components of the local field potential. *Journal of Neuroscience, 31*(25), 9390–9403.

Kilpatrick, Z., & Ermentrout, B.E. (2011). Sparse gamma rhythms arising through clustering in adapting neuronal networks. *PLOS Computational Biology,* to appear.

Krupa, M., & Szmolyan, P. (2001). Extending singular perturbation theory to nonhyperbolic points – fold and canard points in two dimensions. *SIAM Journal on Mathematical Analysis, 33*, 286–314.

von Stein, A., & Sarnthein, J. (2000). Different frequencies for different scales of cortical integration: from local gamma to long range alpha/theta synchronization. *International Journal of Psychophysiology, 38*(3), 301–13.

Stiefel, K.M., Gutkin, B.S., Sejnowski, T.E. (2009). The effects of cholinergic neuromodulation on neuronal phase-response curves of modeled cortical neurons. *Journal of Computational Neuroscience, 29*, 289–301.

Tallon-Baudry, C., Bertrand, O., Peronnet, F., Pernier, J. (1998). Induced gamma- band activity during the delay of a visual short-term memory task in humans. *Journal of Neuroscience, 18*, 4244–4254.

Vida, I., Bartos, M., Jonas, P. (2006). Shunting inhibition improves robustness of gamma oscillations in hippocampal interneuron networks by homogenizing firing rates. *Neuron, 49*, 107–117.

Wang, X.J. (2010). Neurophysiological and computational principles of cortical rhythms in cognition. *Physiology Review, 90*, 1195–1268.

Whittington, M.A., Stanford, I.M., Colling, S.B., Jefferys, J.R.G., Traub, R.D. (1997). Spatiotemporal patterns of gamma frequency oscillations tetanically induced in the rat hippocampal slice. *Journal Physiology, 502*, 591–607.